



**HAL**  
open science

# A submarine morphotectonic analysis combining GIS-based methods and virtual reality: Case study of the low-rate active thrust faulting off Boumerdès (Algeria)

Jacques Déverchère, Antoine Barbé, Maxime Kernec, Marion Jaud, Riwalenn Ruault

## ► To cite this version:

Jacques Déverchère, Antoine Barbé, Maxime Kernec, Marion Jaud, Riwalenn Ruault. A submarine morphotectonic analysis combining GIS-based methods and virtual reality: Case study of the low-rate active thrust faulting off Boumerdès (Algeria). *Frontiers in Earth Science*, 2022, 10, pp.Article number 1010226. 10.3389/feart.2022.1010226 . hal-04157826

**HAL Id: hal-04157826**

**<https://hal.univ-brest.fr/hal-04157826>**

Submitted on 10 Jul 2023

**HAL** is a multi-disciplinary open access archive for the deposit and dissemination of scientific research documents, whether they are published or not. The documents may come from teaching and research institutions in France or abroad, or from public or private research centers.

L'archive ouverte pluridisciplinaire **HAL**, est destinée au dépôt et à la diffusion de documents scientifiques de niveau recherche, publiés ou non, émanant des établissements d'enseignement et de recherche français ou étrangers, des laboratoires publics ou privés.



Distributed under a Creative Commons Attribution 4.0 International License



## OPEN ACCESS

## EDITED BY

Nibir Mandal,  
Jadavpur University, India

## REVIEWED BY

Puspendu Saha,  
Indian Institute of Technology Kanpur,  
India  
Subhajit Ghosh,  
University of Orléans, CNRS, France

## \*CORRESPONDENCE

Jacques Déverchère,  
✉ jacdev@univ-brest.fr

## SPECIALTY SECTION

This article was submitted  
to Solid Earth Geophysics,  
a section of the journal  
Frontiers in Earth Science

RECEIVED 02 August 2022

ACCEPTED 13 December 2022

PUBLISHED 23 December 2022

## CITATION

Déverchère J, Barbé A, Kernec M,  
Jaud M and Ruault R (2022), A  
submarine morphotectonic analysis  
combining GIS-based methods and  
virtual reality: Case study of the low-rate  
active thrust faulting off  
Boumerdès (Algeria).  
*Front. Earth Sci.* 10:1010226.  
doi: 10.3389/feart.2022.1010226

## COPYRIGHT

© 2022 Déverchère, Barbé, Kernec,  
Jaud and Ruault. This is an open-access  
article distributed under the terms of the  
[Creative Commons Attribution License  
\(CC BY\)](https://creativecommons.org/licenses/by/4.0/). The use, distribution or  
reproduction in other forums is  
permitted, provided the original  
author(s) and the copyright owner(s) are  
credited and that the original  
publication in this journal is cited, in  
accordance with accepted academic  
practice. No use, distribution or  
reproduction is permitted which does  
not comply with these terms.

# A submarine morphotectonic analysis combining GIS-based methods and virtual reality: Case study of the low-rate active thrust faulting off Boumerdès (Algeria)

Jacques Déverchère<sup>1\*</sup>, Antoine Barbé<sup>1</sup>, Maxime Kernec<sup>2</sup>,  
Marion Jaud<sup>1,3</sup> and Riwalenn Ruault<sup>2</sup>

<sup>1</sup>Geo-Ocean, Univ Brest, CNRS, Ifremer, UMR6538, Plouzané, France, <sup>2</sup>EUR ISblue, IUEM, Brest, France, <sup>3</sup>CNRS, Pôle Image et Instrumentation, UAR 3113, IUEM, Univ Brest, Plouzané, France

The Algerian margin is located at the slow-rate convergent boundary between African and Eurasian plates and experienced several strong earthquakes in the last centuries. Among them, the 2003 Mw 6.8 Boumerdès event has triggered large turbidity currents in the slightly concave canyons of the slope and numerous cable breaks in the abyssal plain. In this study, we explore where, how and when the tectonic inversion of the margin off Boumerdès has left witnesses in the seafloor morphology and whether the observed deformation correlates with the 2003 coseismic rupture zone and with the Plio-Quaternary sedimentation. We have performed a careful analysis of the seafloor morphology and subsurface seismic reflectors at the landscape scale and along/between canyons by combining classical GIS-based methods and Virtual Reality techniques. From the mid-slope to the deep basin off the ~60 km long Boumerdès-Dellys coast, we evidence large knickpoints corresponding to the development of four main cumulative fault scarps and two perched basins which are deeply incised by steep canyons and gullies. We interpret these structures to result from frontal propagation of two main south-dipping thrusts by upper crustal décollement ramping, evidencing an incipient sub-thrust imbrication in a stage of initiation of an accretionary wedge. The flat-ramp thrust geometry and their along-strike segmentation explain the development and shape of the perched basins in the backlimb of fault-related folds. The onset of growth strata is dated at  $1.5 \pm .5$  Ma on the slope and  $.9 \pm .3$  Ma in the deep basin. The length, position, strike and segmentation of the older, southern thrust ramp are consistent with the coseismic characteristics of the Mw 6.8 2003 earthquake. The cumulative vertical scarp throw exceeds 1 km, supporting Quaternary shortening rates of  $1.6 \pm .7$  mm/yr, in agreement with geodetic strain rates across the western Mediterranean basin. Virtual Reality offers powerful and promising means to correlate seismic imagery and seafloor morphology and is of great help to improve the robustness of tectonostratigraphic interpretation.

## KEYWORDS

submarine morphotectonics, knickpoints, cumulative scarps, boumerdès earthquake, fold-bend faults, inverted passive margin, virtual reality, fault segmentation and growth

## 1 Introduction

Submarine geomorphology of continental margins results from numerous competing processes arising from erosion, gravity, currents and tectonics. The identification of cumulative and single-event deformations at the seafloor (e.g., fault scarp height variations, cumulative fault throws, slide size/distribution and fold/fault strikes and lengths) is important to assess the extent and potential impact of large events (tsunamis, earthquakes, gravity slides) and thus better anticipate their effects on structures such as industrial sites, buildings, submarine cables or offshore platforms, especially in urbanized coastal areas.

In many convergent margins settings (subduction zones), the record of active deformation at the seafloor is often well preserved and provides compelling evidence of complex interactions between these competing processes (see e.g. Graindorge et al., 2008; Polonia et al., 2011; Gutscher et al., 2017; Morgan et al., 2022 and references therein). By contrast, the tectonic reactivation of passive margins leads to much more tenuous witnesses of faulting and folding at the ocean-continent transition, at least in early stages, owing to the highly variable autogenic and allogenic controls on submarine landscapes (Pratson et al., 2007; Pettinga and Jobe, 2021) in a context of comparatively lower strain rates and widespread deformation (e.g. Auzemery et al., 2021; Somoza et al., 2021).

Among the rare examples of reactivated passive margins, the Algerian margin case study has received a peculiar attention in the last 20 years. Indeed, this margin illustrates a typical case of a weak mantle lithosphere with short length-scales of deformation (Hamai et al., 2015; Auzemery et al., 2021) and

locates at a diffuse plate boundary which absorbs most of the slow convergence between Africa and Europe (Palano et al., 2015; Bougrine et al., 2019; Serpelloni et al., 2022; Billi et al., 2023), producing rare but strong, sometimes damaging earthquakes (Hamdache et al., 2010; Bellalem et al., 2022). The 1856, 1954, 1980 and 1985 earthquakes (Figure 1) are among the main historical and instrumental earthquakes worth to mention. More recently, the scientific community has realized after the occurrence of the 2003 May 21 Mw 6.8 Boumerdès earthquake that a major south-dipping thrust fault is located below the central Algerian margin, eastward Algiers capital City (Figure 1), with an epicenter close to the coastline (Delouis et al., 2004; Belabbès et al., 2009; Ouyed et al., 2011). This event has caused the death of more than 2,300 people and severe damage in a large coastal zone around Boumerdès (Ayadi et al., 2003). The successive marine surveys launched in the following years have evidenced the huge submarine impact of this earthquake in terms of turbidity currents and telecommunication cable breaks (Cattaneo et al., 2010). It has also led to a controversy regarding the exact position and geometry of the thrust fault system when approaching the surface: while some authors propose that a “ramp-on-flat” hanging wall - footwall configuration may explain why a major slope break is shifted northward relative to the rupture zone (Déverchère et al., 2005; 2010; Strzeczynski et al., 2010; 2021; Kherroubi et al., 2017), other ones claim that the active thrust remains essentially planar upwards and would reach the seafloor (or subsurface) close to the continental shelf edge or in the upper slope (Ayadi et al., 2008; 2010; Belabbès et al., 2009).

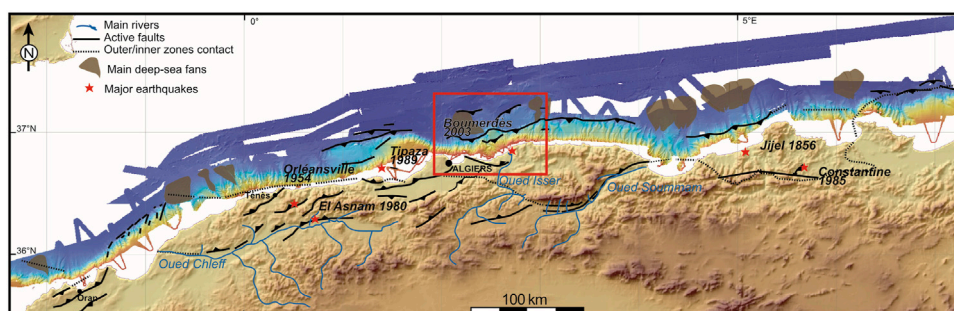


**FIGURE 1**

Overall land-sea physiography and structural sketch of the Algerian margin, with the six major earthquakes (red stars) felt since 1850. Main rivers and deep-sea fans are shown. Black lines show the approximate position of the main active faults close to the surface. Dashed line is the assumed position of the suture zone corresponding to the closure of the Tethyan (Maghrebian) oceanic lithosphere. Red square is the study area where the Mw 6.9 May 2003 Boumerdès earthquake occurred. Modified after Bouillin (1986), Domzig et al. (2006), Yelles-Chaouche et al. (2006) and Cattaneo et al. (2010).

In this paper, we seek to review the existing potential imprints of recent and active cumulative deformation, both at the seafloor and in structures at depth of the central Algerian margin (Algiers-Boumerdès region, [Figure 1](#)), using a combination of classic Geographical Information System (GIS) and Virtual Reality (VR) methods. Indeed, several recent studies have evidenced the potential of an immersive VR experience to improve geological analyses of outcrops on land or at sea without temporal or spatial limitations and in a more interactive way, either for research or for geo-education purposes (e.g., [Billant et al., 2019](#); [Bonali et al., 2022](#); [Jaud et al., 2022](#)). Our aims are: 1) to clarify the debate on the Boumerdès fault outcrop at the seafloor, 2) to reveal the potential of VR applied to the visualization of submarine structures at the landscape scale in order to highlight the possible role of geometrical changes of thrust faults in the surface expression of tectonics, and 3) to discuss the consistency of strain indicators in this peculiar case of slow-rate inversion of a Cenozoic passive margin.

## 2 Geological and seismotectonic settings

### 2.1 Geological setting and turbiditic regime

Geology of northern Algeria results from a succession of geodynamic events that occurred within the framework of the Africa-Eurasia plate convergence. Tethyan (Maghrebian) slab subduction occurred from ~30 Ma to ~19 Ma, forming the Liguro-Provençal basin by southward rollback, until the collision of the Kabylides (Kabylid blocks) with the African continent ([Bouillin, 1986](#)). Later on (~18–8 Ma), bilateral slab tearing and continental mantle delamination have triggered the thermal erosion of the continental mantle ([Abbassene et al., 2016](#); [Chazot et al., 2017](#)) and the reworking and development of the present-day Algero-Balearic basin ([Haidar et al., 2022](#), and references therein). Finally, the Africa-Eurasia convergence has resumed the orogenesis of the Atlas and enhanced the progressive tectonic inversion of the Algerian margin towards the north since ca. 8 Ma ([Recanati et al., 2019](#); [Lefondré et al., 2021](#)). Before this last stage, a major paleo-environmental event called the Messinian Salinity Crisis (MSC) gave birth to the deposition of thick layers of evaporites in the deep basins and the margin and to specific seismic markers, sedimentary units and structures ([Lofi et al., 2011](#); [Roveri et al., 2014](#); [Dal Cin et al., 2016](#), and references therein). Basins bordered by high reliefs and steep slopes without large continental shelves have accumulated abundant clastic sediments at the margin toes during the deposition of Messinian salt and upper evaporites, as reported in the Ligurian sea ([Savoie and Piper, 1991](#); [Sage et al., 2011](#)) and in the Algerian margin ([Déverchère et al., 2005](#); [Capron et al., 2011](#)). Since Pliocene time, high-stand stacked prograding

systems tracts resting upon a major erosional surface have emplaced in upper margins, while lower slopes and deep basins have hosted large deep-sea fans ([Figure 1](#)) and a succession of turbiditic and hemipelagic layers ([Giresse et al., 2009](#); [Babonneau et al., 2012](#); [2017](#)).

At least during the highstand period, the bimodal periodicity of turbidites is likely controlled by the occurrence of large earthquakes whose sources are close to the coastline ([Giresse et al., 2009](#); [Ratzov et al., 2015](#)). The cable breaks following the 2003 Mw 6.8 Boumerdès earthquake ([Ayadi et al., 2003](#); [Cattaneo et al., 2010](#)) and the 1954 M 6.7 Orléansville earthquake ([Heezen and Ewing, 1955](#)) support this interpretation and show that earthquake-induced turbidity currents have the potential to affect deep and remote areas around the rupture zones ([Cattaneo et al., 2010](#)).

### 2.2 Coseismic and interseismic deformation

Great attention has been paid to the seismotectonic setting of the Boumerdès region after the 2003 May 21 Mw 6.8 earthquake. Like most large aftershocks, this event displays pure reverse faulting with the maximum stress axis striking ~N160°E, i.e. sub-parallel to the mean regional stress direction ([Kherroubi et al., 2017](#)). Although the source models constrained by seismological and geodetic observations are numerous and slightly differ between each other ([Belabbès et al., 2009](#)), there is a general agreement to consider that as a whole, the seismogenic fault strikes N60–70°E, dips ~40°–45° toward the SE and locates offshore about 8–13 km from the coastline ([Delouis et al., 2004](#); [Meghraoui et al., 2004](#); [Ayadi et al., 2008](#); [Mahsas et al., 2008](#); [Belabbès et al., 2009](#); [Kherroubi et al., 2017](#); [Beldjoudi and Delouis, 2022](#); [Figure 2](#)). Nevertheless, most source and local tomography models point to a clearly segmented fault rupture: indeed, aftershocks in the footwall delineate a surface matching the position and dip of the main rupture plane, with a western patch at 7–15 km depth dipping ~40°SE and an eastern patch at 8–20 km depth dipping ~20° SE ([Kherroubi et al., 2017](#)). This segmentation is also found both in the two coseismic slip patches of the main rupture at ~10 and ~5 km depth west and east respectively ([Delouis et al., 2004](#); [Belabbès et al., 2009](#); [Beldjoudi and Delouis, 2022](#)) and in the afterslip model within the 2.5 years after the earthquake ([Mahsas et al., 2008](#)).

Finally, continuous geodetic (GNSS) measurements in Africa and Europe highlight the interseismic strain rate distribution between northern Algeria and the Balearic promontory ([Serpelloni et al., 2007](#); [2022](#); [Bougrine et al., 2019](#); [Sparacino et al., 2020](#); [Billi et al., 2023](#)). They show that 1) geodetic velocity vectors relative to Eurasia strike roughly NW-SE and decrease progressively in length from west (~3.0 mm/yr) to east (~.5 mm/yr) along the coast of Algeria, and 2) the horizontal shortening

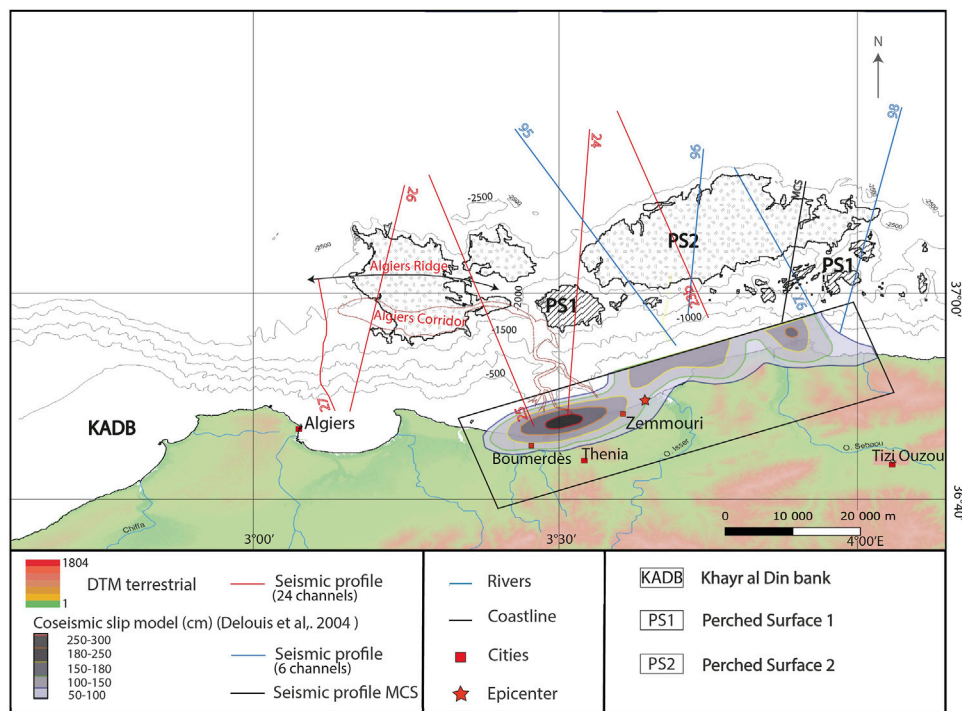


**FIGURE 2**

Map of the Boumerdès area displaying the position of the seismic sections used in this study and the contours of the two flat surfaces PS1 and PS2 identified under GIS (see also Figure 3). Mean position of the 2003 May 21 rupture plane (projected in map view) is also shown as a thin black rectangle, after Delouis et al. (2004). This fault model makes the hypothesis of a single rupture plane ~60 km long and ~24 km wide extending from the surface to a depth of ~17 km. The grey contour lines inside the rupture plane displays the coseismic slip values in centimeters. Red dotted line locates the position of the Algiers canyon and corridor (Babonneau et al., 2017). MCS: Multichannel Seismic Section from the industry (Déverchère et al., 2005).

rate in the offshore domain is of about 1.5 mm/yr at the longitude of Boumerdès. Therefore, the long-term horizontal slip rate on the Boumerdès fault is necessarily less than this value since there is evidence for some continuous deformation (likely lower than 20%) by buckling of the oceanic lithosphere (Lefondré et al., 2021) and because some NW-SE shortening is also taking place at the toe of the Balearic margin (Camerlenghi et al., 2009; Maillard and Mauffret, 2013; Blondel et al., 2022).

### 3 Data and methods

Sediment transport on continental slopes is controlled by turbidity currents, submarine landslides, debris flows and contourites (e.g., Ercilla et al., 2022): they form various markers (canyons, channel-levees, slide scars, slope breaks, knickpoints) on which tectonic activity may superimposed, such as cumulative scarps, perched surfaces or basins, folds, often well expressed in thrust belts (Suppe, 1983). They can thus be identified by a geomorphic analysis and the use of seismic sections in the areas where erosion is less pronounced.

### 3.1 Datasets used

For the purpose of this study, we benefited from a set of bathymetric and seismic data acquired on board Research vessel *Le Suroît* in the period 2003–2005 during the MARADJA (<https://doi.org/10.17600/3020100>) and MARADJA2/SAMRA cruises (<https://doi.org/10.17600/5020080> and <https://doi.org/10.17600/5020090>). For bathymetry, we have used Kongsberg EM300 (for the slope and deep basin) and EM1000 (for the continental shelf) Simrad multibeam echosounders. Data processing was made with the Caribes<sup>®</sup> software, allowing us to produce a Digital Elevation Model (DEM) with the resolution of 25–35 m (depending on depth) for our study zone (Figure 2). We have also gathered coastal bathymetric data digitized from Leclaire (1970)'s bathymetric maps. During the 2003 and 2005 cruises, seismic reflection data were obtained by either six- or 24-channel streamers using a combination of two and six double chamber gas-injection air-guns. We have used the SU (Seismic Unix) CWP/SU software (Center of Wave Phenomena, Colorado School of Mines) for the stack and migration of the seismic data, complemented by some previously published seismic lines of the Algerian Oil Company (Déverchère et al.,

2005). All the data used in this study have been previously the object of analyses and interpretation. We have merely re-used the same data in a new visualization environment and in an enriched framework of analysis (especially regarding the longitudinal profiles in canyons). Until now, the data sets available off Boumerdès were not explored this way.

### 3.2 Methods of geoscientific visualization and data analysis

On land, remote sensing techniques provide since long the possibility to capture the small scale topographic roughness thanks to DEMs of high spatial resolution, thus encouraging the use of new tools such as VR for virtual geological exploration of the morphology and a quality control on structural measurements (e.g., Nesbit et al., 2020; Jaud et al., 2022). Until now, such virtual explorations are rarely performed under the sea because data resolution is often too low and because free tools available to explore the richness of datasets by VR techniques (beyond the seafloor morphology alone) are yet limited (e.g., Métois et al., 2021; Billant et al., 2019, and references therein). However, submarine environments appear to benefit from several advantages to preserve the record of geological events, such as low erosional rates, continuous sedimentation in time and space and limited impacts by human activities (Perea et al., 2021). Furthermore, the recent development of instruments for multiscale seafloor mapping and sub-seafloor seismic imaging allows us to improve year after year the spatial coverage, the resolution and the accuracy of the data, at least in some specific zones.

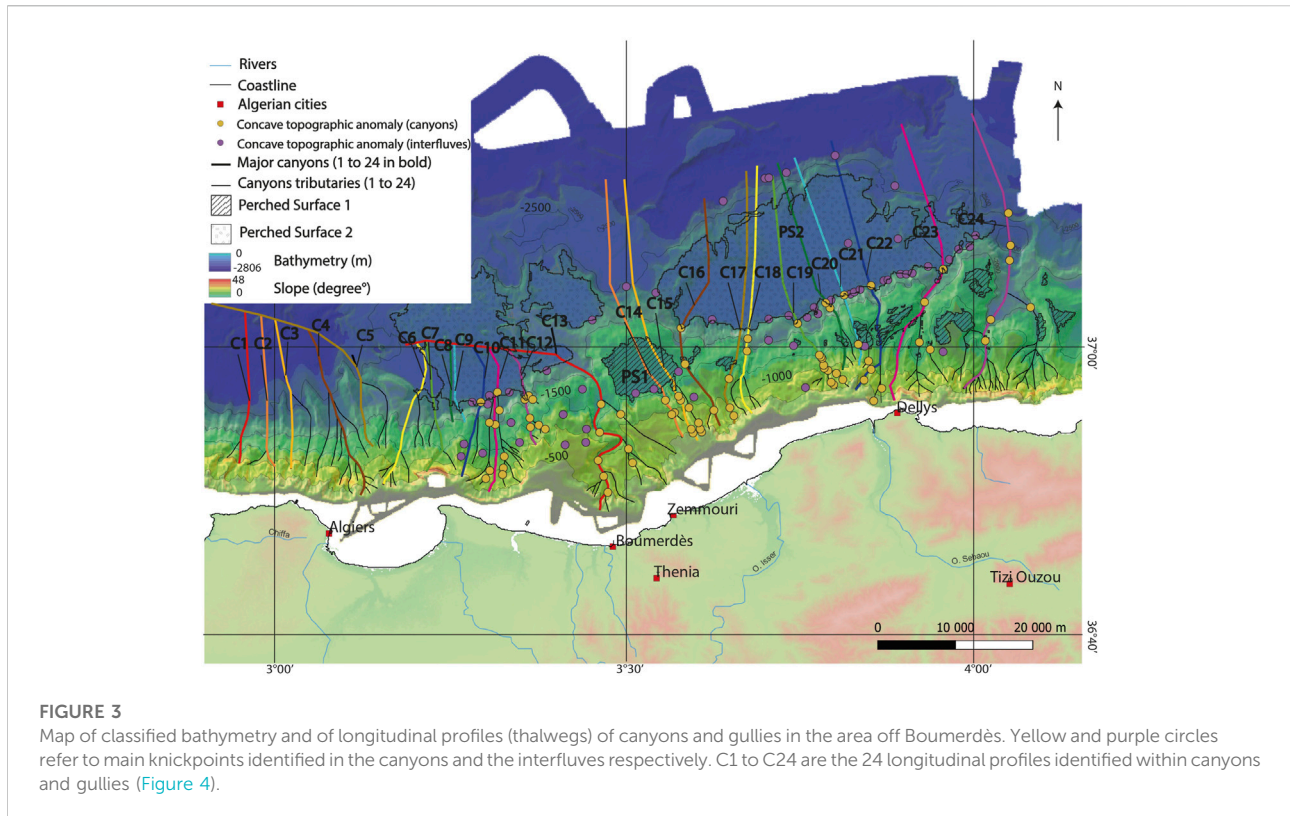
In our study area (Figures 1, 2), a first analysis has been performed using classic GIS tools (QGIS and ArcGIS), in particular to digitize canyon thalwegs and extract bathymetric profiles along these thalwegs. To complement this GIS approach, a Virtual Reality (VR) environment was built using the platform Unity (<https://unity.com/>) for real-time content creation. For the DEM exploration, we use the free Unity package (including ArcGIS Maps SDK plugin) and an Oculus Quest headset, with touch controllers, including GIS-like interaction capabilities, as also done by Billant et al. (2019), allowing the user to move freely within a 3D immersive environment. We have also developed specific tools for the purpose of this study, such as superimposition in real time of various layers as backscattering imagery and DEMs. An originality of our VR approach consisted in adding 2D data in a vertical plane, which cannot be represented in a classical GIS, such as seismic reflection profiles. These seismic sections can be loaded above or below the seafloor, with the possibility of adjusting the vertical exaggeration of seismic sections during the “virtual dives”. We have performed successive periods of VR sessions called “immersions” limited to 2 h. They allow for a three-dimensional, 360° and multi-scale exploration of the whole data set at the same time and the easy

superimposition in three dimensions of the surface and sub-surface markers, and thus offer the user a much better accessibility to the erosional, depositional and tectonic processes acting on the central Algerian slope and deep basin. The user is also equipped with a laser pointer (located on the joysticks) that allows him to locate points of interest and interact with other users, facilitating discussions. This pointer also allows the user to draw or annotate information directly in the virtual environment, which was especially useful to interpret seismic profiles. We present as **Supplementary Material S1** (SM) two movies illustrating the interactive navigation in the VR environment using surface (SM1) and sub-surface (SM2) environments. In the near future, we hope that the implementation of new tools in VR (position and depth information; distance/surface/dip measurements; digitalization in the form of shapefile and export) will enrich VR immersions and limit back and forth with GIS.

## 4 Results

### 4.1 Longitudinal profiles inside canyons and gullies

The submarine canyon-and-channel systems are known since long to result from repeated transport of sediments downslope by gravity flows and other mass movements (Menard, 1955; Shepard, 1981; Mitchell, 2005). The relative convexity or concavity of longitudinal profiles have been examined at the world scale by Covault et al. (2011). In our study, we have analyzed the shape of the main canyons and gullies found off Boumerdès and Algiers (Figure 3). We have then compared their shapes and sizes to the groups determined from visual inspection by Covault et al. (2011). We have first examined the profiles west of the Boumerdès rupture zone (from west to east, C1 to C13, Figure 3; Figure 4A). In this area, the slope is characterized by steep gradients (about 8°–10°) incised by numerous gullies. The profiles display almost rectilinear (falling in the “slightly concave” group by Covault et al., 2011) shapes as a whole, without any knickpoints. The three profiles at the western edge (C1 to C3) are the steepest ones: they are linear on the slope and reach -2,700 m depth before becoming flat. Profiles C4 to C12 are also quasi linear on the slope but are slightly less steep and depict a large, asymmetrical bulge ~400 m high and ~20 km wide in the abyssal plain, between -2,300 m and -2,700 m (Figure 4A). Babonneau et al. (2017) have shown that this bulge results from the growth of the Algiers sedimentary deep-sea fan at the outlet of the Algiers canyon. Two south-dipping blind thrusts below the fan form asymmetric anticlines (ridges) bordered by a large perched surface at the margin toe, named the “Algiers corridor” (Figure 2), corresponding to the backlimb of a fold-bend fault (Suppe, 1983). Profiles C1 to C12 crosscut the axis of this corridor, which depicts a gentle



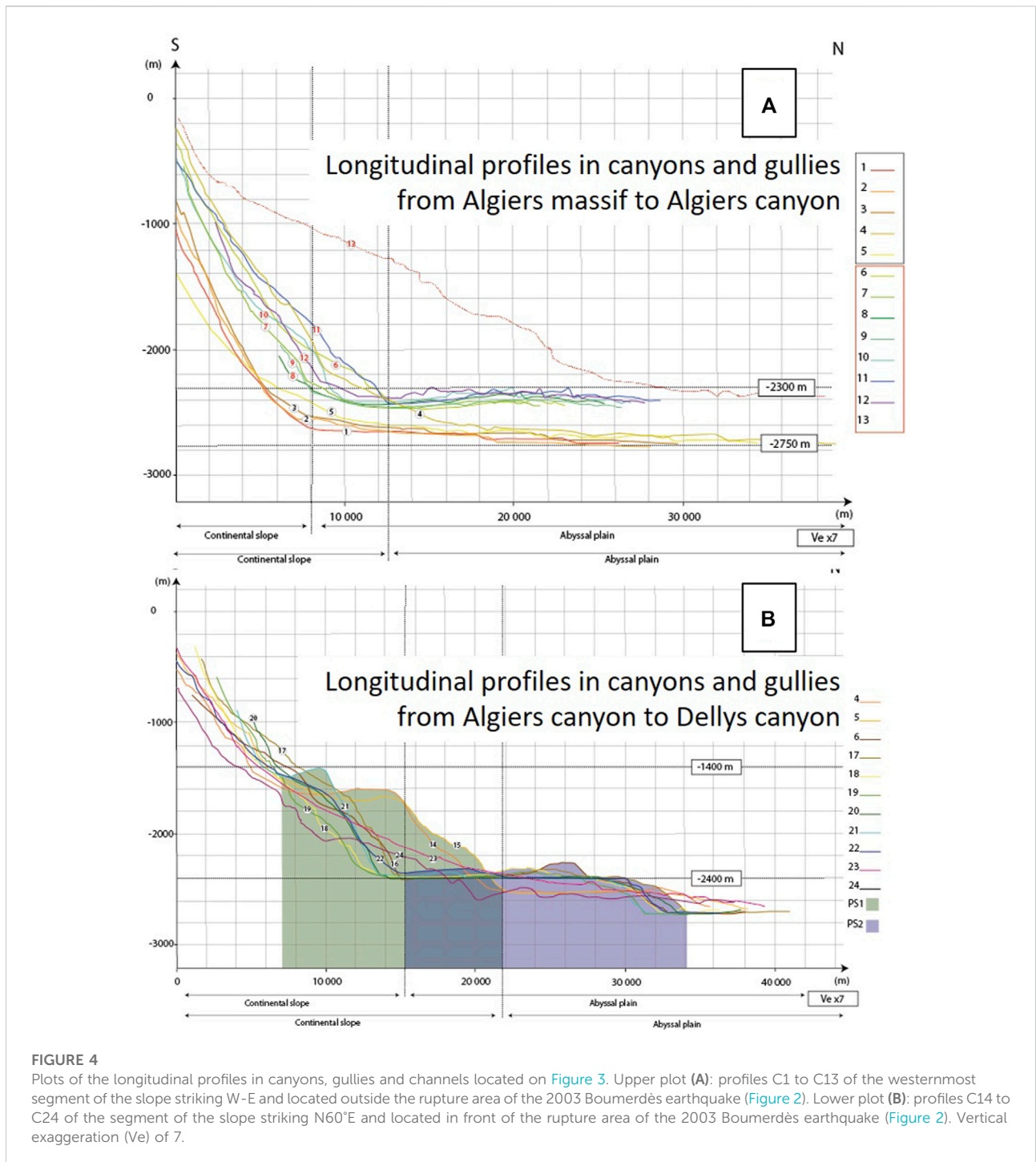
slope towards the west. Only Profile C13 (Algiers canyon and ridge) departs from the general pattern, with a rather regular slope of about  $5^\circ$  down to  $-2,400$  m, except two bulges at km 20 and km 30 (Figure 4B), within the Algiers corridor. Indeed, the Algiers canyon represents the only well-incised canyon of the area, with two main tributaries in its upper part, a strong westward deviation at the foot of the slope and a well-developed channel-levee system in the abyssal plain (Figure 3; Babonneau et al., 2017).

Profiles on the slope corresponding to the 2003 fault rupture (from west to east, C14 to C24, Figure 3; Figure 4B) appear to be strikingly different: the mean slope decreases to  $5\text{--}7^\circ$  and the profiles are also slightly concave but with a major anomaly depending on the longitude: 1) to the west (profiles C14–C15, green area in Figure 4B), a major break occurs at mid-slope (between  $-1400$  and  $-1600$  m), forming a surface of  $2\text{--}6$  km wide (perched surface PS1) slightly tilted toward the south and identified as a large rounded surface in the classified bathymetry (Figure 3); 2) to the east (profiles C16–C24, purple area in Figure 4B), the canyons and gullies depict slightly concave shapes but with many irregularities and knickpoints on the slope down to  $-1400$  m, followed by a relative flat plateau of  $18\text{--}20$  km wide (perched surface PS2). In the deepest part of the basin, the morphology of the seafloor is even more complex, with Messinian salt piercing diapirs and elongated highs and mass transport deposits (Babonneau et al., 2017).

## 4.2 Longitudinal profiles in interfluves and along strike

Interfluvial profiles may help to visualize the major slope breaks in areas preserved from intense erosion. They allow us to check that the topographic anomalies (slope breaks, knickpoints, flat surfaces) described above within the thalwegs (S4.1) are also identified and to compare their size and distribution.

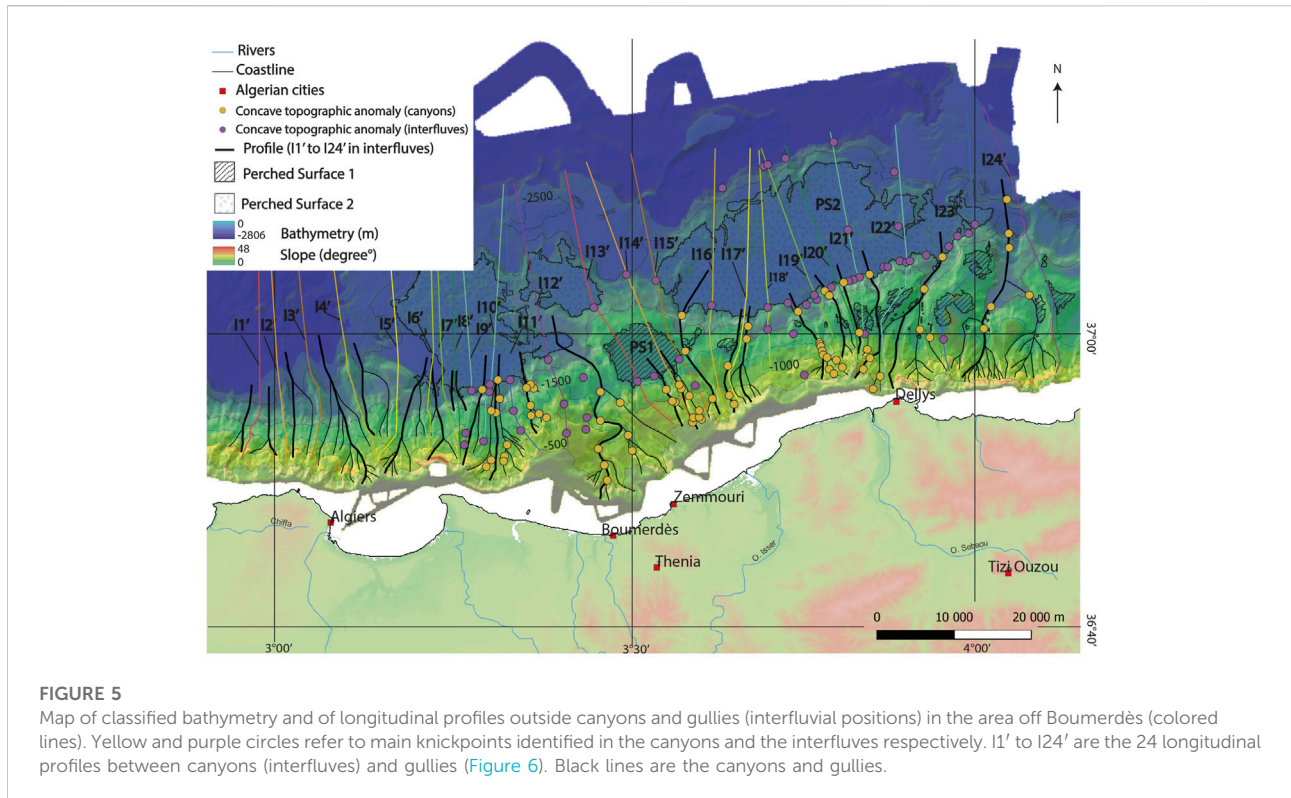
The twelve westernmost profiles (I1' to I12', Figure 5; Figure 6A) display a pattern similar to the one observed with canyons C1 to C12 (Figure 3; Figure 4A): a steep and rectilinear slope but with a higher variability, followed by a wide, asymmetrical bulge  $\sim 400$  m high and  $\sim 24$  km wide in the abyssal plain. To the east, in front of the Boumerdès rupture plane (Figure 5; Figure 6A), profiles I13' to I15' and I22' to I24' underline a major step  $6\text{--}8$  km wide on the slope, between  $-1500 \pm 100$  m and  $-1700 \pm 100$  m respectively, corresponding to the surface mapped as PS1 (Figures 2, 3). The surface to the west is clearly tilted counter slope, as already seen for longitudinal profiles C14 and C15 (Figure 4B). Intermediate interfluvial profiles (I17' to I21') also display a step at similar depths but are either hardly detected (I17' to I19') or very narrow (I20' and I21'). In the abyssal plain, the profiles also evidence large, flat areas (PS2)  $\sim 16$  km wide and  $\sim 300$  m high for profiles I17' to I21' and of  $10\text{--}14$  km wide and  $\sim 200$  m high for other profiles.



Finally, we use the alignments of knickpoints along strike (colored circles in Figure 3; Figure 5) to evidence the lateral changes in depths of the two main concave slope breaks that limit surfaces PS1 and PS2 oceanwards (Figure 7). Although short wavelength irregularities disturb the profiles, in relation both to differential erosion at the outlets of canyons and to the numerous landslides identified (Dan et al., 2009; 2010; Cattaneo

et al., 2010), the two profiles depict the same general pattern, i.e. a clear deepening from west to east, reaching amplitudes of ~700 m and ~400 m for PS1 and PS2 limits, respectively. While the depth change is rather progressive for PS2, it appears to be abrupt for PS1, delineating a western plateau ~27 km long at -1600 m depth and an eastern surface ~25 km long at -2,300 m depth. Note that the length, strike, longitudinal position and segmentation (2 parts of similar





length but shifted of about 700 m) of the red curve (PS1) match quite well the ones of the 2003 Mw 6.8 rupture fault model of the Boumerdès earthquake, which also displays two main slip patches in a similar position along strike (Figure 2; Delouis et al., 2004; Belabbès et al., 2009; Beldjoudi and Delouis, 2022). Thanks to the Virtual Reality tools developed in this project, we have explored at different scales and in 3D navigation the morphological expression of these slope breaks (Figure 7; SM1): they appear to represent the two main morphological anomalies at the seafloor, dominating the other seafloor signatures that appear to be spatially much more limited or spread in space (e.g., sediment waves, levees, slide scars, salt diapirs or salt walls, see Dan et al., 2009; 2010; Cattaneo et al., 2010; Babonneau et al., 2017). Furthermore, we have checked that the perched surfaces PS1 and PS2 are also gently dipping eastward. Using a combined visualization of backscattering and DEM images in VR (SM1), we were also able to evidence the present-day activity of the canyons and the “fresh” and irregular pattern of scarps F1 and F2 in the interfluves, testifying that these scarps represent surface expressions of a significant tectonic deformation.

#### 4.3 Onset and timing of tilted perched basins

Non-planar faults are commonly observed worldwide in fold-thrust belts and are called fault-bend faults (Suppe, 1983). As a

result of changes in fault geometry, a distortion occurs in the hanging wall of the fault above the place where the fault steps up in the direction of slip to a higher décollement or to the surface. It results in the birth of a perched basin in the backlimb of the fold and may also produce imbricate fold-bend folds and fault-propagation folds outward. Depending on the geometry of the master fault and the amount of displacement, these basins are called wedge-top basins (Leprêtre et al., 2018), rollovers (Xiao and Suppe, 1992) or piggy-back basins (Ori and Friend, 1994), and are associated with a listric normal fault flattening at depth. Off Boumerdès, growth strata and tilted sediments have been reported for long and were initially interpreted as extensional tilted blocks of a stretched continental margin, and later on as resulting from thrust ramps of the passive margin inversion (Déverchère et al., 2005; Domzig et al., 2006; Strzeczynski et al., 2010; Capron et al., 2011). In order to explain the position and geometry of the two basins identified on the slope (Figures 8, 9), these authors have proposed a ramp-flat-ramp geometry of the active fault near the surface, with a basal flat below the upper basin and a shallower flat below the lower basin, followed by a frontal ramp. Thanks to the potentiality of the VR environment (SM1 and SM2), we show here the clear link between morphological anomalies reported (perched surfaces mapped on Figures 2, 3; Figure 5 and longitudinal profiles of Figure 4; Figure 6) and tilted sedimentary units. For simplicity, we name here the basins “perched basins” (PB), since they appear to be settled above the abyssal plain (maximum values of +1300 m and +300 m for PS1 and PS2 respectively, Figure 4; Figure 6).

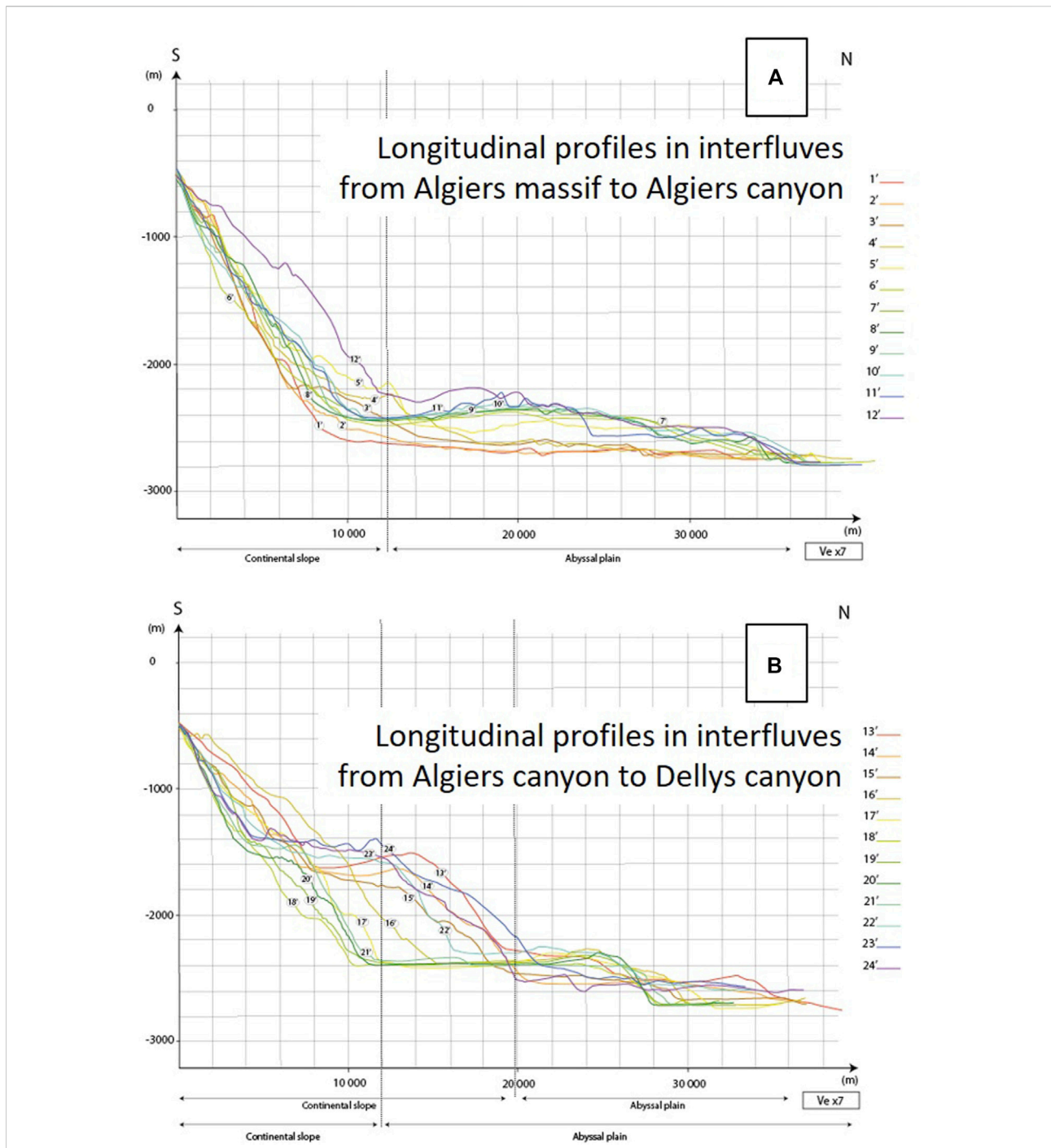


**FIGURE 6**  
 Plots of the longitudinal profiles outside canyons (interfluvial) located on Figure 5. Upper plot (A): profiles 1' to 12' of the westernmost segment of the slope striking W-E and located outside the rupture area of the 2003 Boumerdès earthquake (Figure 2). Lower plot (B): profiles 13' to 24' of the segment of the slope striking N60°E and located in front of the rupture area of the 2003 Boumerdès earthquake (Figure 2). Vertical exaggeration (Ve) of 7.

The first perched basin downslope (PB1) is expressed at the seafloor by a patchwork of small surfaces (Figure 2), suggesting that they result from the incision by numerous active canyons

(C13 to C24, Figure 3). We repeat the same analysis for the second perched basin downslope (PB2), expressed by large surfaces (“plateaus”) extending about 300–400 m above the

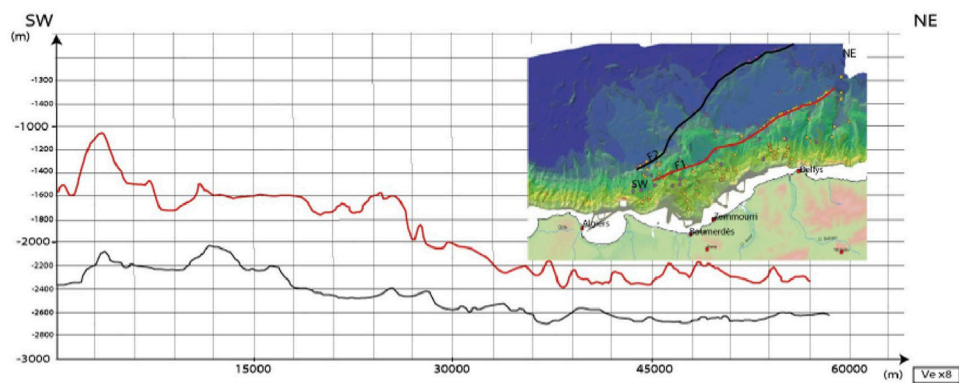


**FIGURE 7**  
 Along-strike topographic profiles following the two main concave slope breaks (continuous morphological scarps) identified by alignments of knickpoints (yellow and purple circles for knickpoints identified in the canyons and the interfluves, respectively). Upper curve (red) is taken at the foot of the scarp interpreted by Déverchère et al. (2005; 2010) as the blind thrust ramp (F1) in the prolongation of the 2003 rupture plane. Lower curve (black) is where several studies have reported the existence at depth of a south-dipping thrust ramp (F2; Déverchère et al., 2005; Dornzig et al., 2006; Strzeczynski et al., 2010). Vertical exaggeration (Ve) of 8. See text for details.

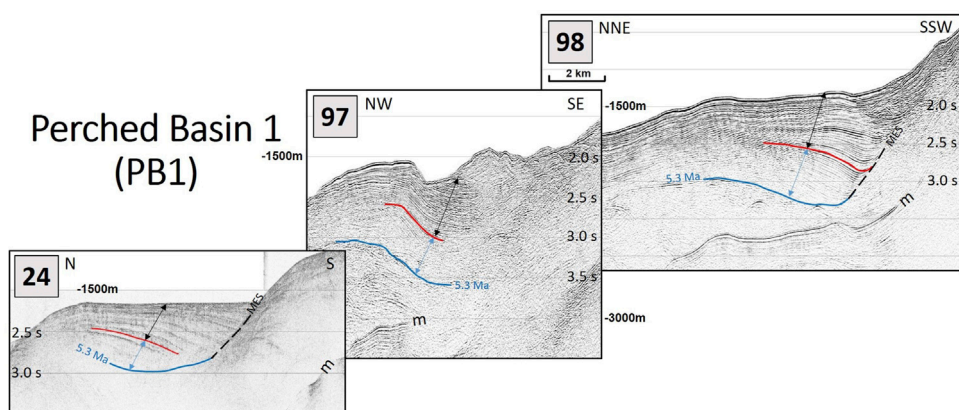


**FIGURE 8**  
 Two-way travel time seismic sections (zooms) 24, 97, 98 from west to east off Boumerdès, displaying growth strata below the perched surfaces PS1. Zooms are located on Figure 2. Double black arrows: sedimentary unit interpreted as growth strata (wedges), assumed to be synchronous to tectonic inversion by thrust ramps. Double blue arrows: sedimentary unit assumed to be deposited prior to the onset of tectonic inversion. Arrows are placed in order to represent the mean thickness of the depocentres. Red line marks the limit between the two sedimentary units, i.e. time when tectonic deformation began. Faults responsible for growth strata development in the hanging wall are south-dipping blind thrusts and are not imaged here owing to moderate penetration. Spacing between horizontal lines is 500 m two-way travel times. M = first multiple of the seafloor. MES = Margin Erosion Surface (Lofi et al., 2011), a polygenic erosional surface interpreted to represent the entire time interval of the drawdown phase of the Messinian Salinity Crisis. See text for details.

deep basin floor (Figure 2; Figure 5; Figure 6). Six section extractions (24, 97, 98 for PB1; 23b, 96, 97 for PB2, from west to east) of moderate to high resolution allow us to image the depositional pattern of these two basins along strike off Boumerdès (Figures 8, 9). All profiles depict clear growth strata in the upper sedimentary pile tilted towards the upper margin and limited abruptly upslope by a reflector dipping

basinward. Basin width coincides with the width of the perched surface 1 (PS1) described above (Figure 2; Figure 5; Figure 6). We use the Messinian marker at the base of the Plio-Quaternary pile (blue line, Figures 8, 9) to identify the base of the oldest deposits. In the deepest basin (PB2), this marker displays undulations interpreted as Messinian salt domes or diapirs resulting from gravity gliding (Déverchère et al., 2005;

## Perched Basin 2 (PB2)

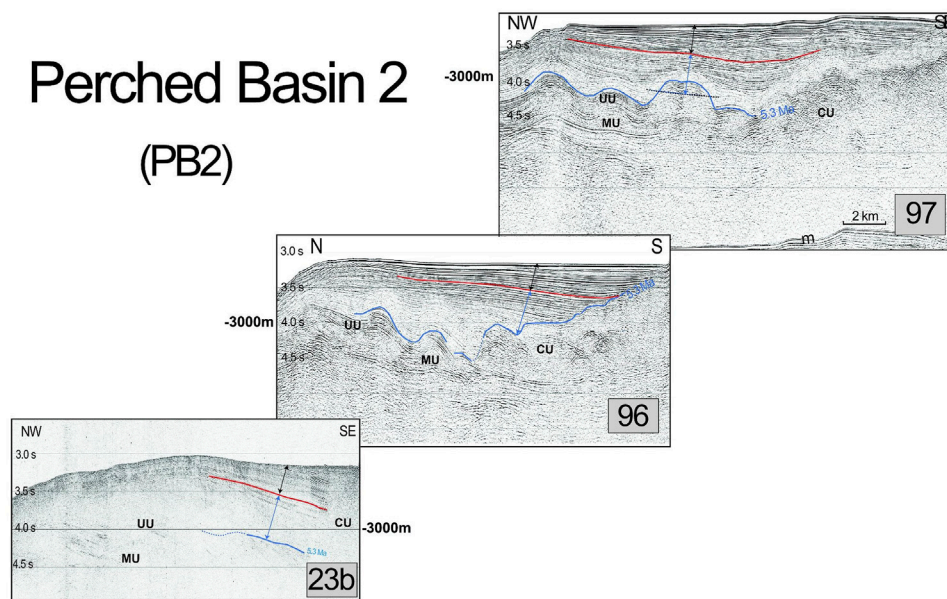


**FIGURE 9**

Two-way travel time seismic sections (zooms) 23b, 96, 97 from west to east off Boumerdès, displaying growth strata below the perched surfaces PS2. Zooms are located on Figure 2. Same caption as in Figure 8. Because of salt tectonics (MU = Mobile Unit), we choose to place the double arrows at locations above Messinian chaotic units (CU) or where the doming is minimal. For Profile 97, we use the half-mean height of the salt dome as reference in order to estimate the PGS thickness.

Strzeczynski et al., 2010; Capron et al., 2011; Babonneau et al., 2017).

By contrast with the Alboran sea (Martinez-Garcia et al., 2013), no chronostratigraphy of the Plio-Quaternary is available owing to the scarcity of log information from wells (Cope, 2003). Although the sediment accumulation rates vary in both time and space between .2 and .6 mm/yr near the margin toe (Giresse et al., 2009; Martinez-Garcia et al., 2013), there is a trend for Pliocene and Quaternary rates to remain relatively homogeneous. From the analyses led by these authors, we may hypothesize average accumulation rates near the foot of the slopes of  $400 \pm 100$  and  $200 \pm 100$  m/Ma for the Quaternary and Pliocene time spans, respectively. Note that these rates have not been decompacted and hence are minimum values. Far inside the deep Algerian basin, the Plio-Quaternary accumulation rate is of 110 m/Ma according to the DSDP drills (Hsü et al., 1973).

In order to check that these average values are realistic, we compute a predicted age of the reflector at the base of the Plio-Quaternary unit when identified on the profiles (Figures 8, 9; Table 1) following the approach proposed by Kherroubi et al. (2009) in the eastern Algerian margin. Although uncertainties are rather large, the mean age found (5.35 Myr) is very close to the age of the reflector marking the lowermost Pliocene (blue line, Figures 8, 9). Therefore, we apply this extrapolation to compute a mean age of the onset of thrust faulting (Table 1) by considering all the seismic lines outside the incised zones and with similar resolution. For PB1 (Figure 2;

Figure 8), we have made independent estimates for three sections (MDJS24, 97, 98): assuming a constant sedimentation rate and neglecting differential compaction, we hypothesize an approximate age for the onset of growth strata at  $1.5 \pm .5$  Ma (Table 1), i.e. Pleistocene. Following the same procedure for PB2 (Figure 2; Figure 9), three sections (MDJS23b, 96 and 97) crossing the deeper basin provide an age of  $.9 \pm .3$  Ma (Table 1). Although uncertainties on these values are rather large owing to the assumptions made and to the disturbances caused by the poor penetration of some lines (MDJS23B and 24) or by salt diapirism which started clearly prior to crustal tectonics (Strzeczynski et al., 2010; Figures 8, 9), the lateral consistency of the results obtained for each perched basin provides some confidence on these values. Furthermore, the average ages predicted for the Plio-Quaternary sequence (5.35 and 5.69 Ma for PS1 and PS2, respectively) are very close to the assumed age of the onset of the modern marine circulation in the Mediterranean estimated between 5.33 and 5.46 Ma (Lofi et al., 2011; Do Couto et al., 2014; Roveri et al., 2014).

### 4.4 Thrust fault heaves

The interfluvial and canyon-gullies longitudinal profiles have evidenced clear morphological anomalies (§4.2, Figures 3–6). We consider these anomalies to be hidden-fault generated because 1) many published seismic sections indeed support that they locate at

**TABLE 1** Thickness of growth strata (GS) and age estimates for the GS onset in perched basins identified off Boumerdès (Figures 8, 9) assuming an interval seismic velocity of  $1.6 \pm 0.2$  km/s and a constant sedimentation rate of  $0.4 \pm 0.1$  mm/yr during Quaternary times. A predicted age of the Plio-Quaternary (PQ) unit is also computed using a constant sedimentation rate of  $0.2 \pm 0.1$  mm/yr during Pliocene times (Martinez-Garcia et al., 2013). Pre-growth strata (PGS) thickness is computed assuming an average seismic velocity of 2.2 km/s. Values of average thicknesses of GS and PGS units are taken from Figure 8; Figure 9 (double black and blue arrows, respectively).

| Profile     | Perched basin | GS average thickness (ms) | GS average thickness (m)       | GS onset predicted age (Ma)     | PGS average thickness (ms) | PGS average thickness (m) | PGS predicted duration (Ma)     | Pq predicted age (Ma)             |
|-------------|---------------|---------------------------|--------------------------------|---------------------------------|----------------------------|---------------------------|---------------------------------|-----------------------------------|
| MDJS24      | <b>PS1</b>    | 560                       | $450 \pm 60$                   | $1.24 \pm .46$                  | 400                        | 440                       | $2.94 \pm 1.47$                 | $4.18 \pm 1.93$                   |
| MDJS97      |               | 700                       | $560 \pm 70$                   | $1.52 \pm .54$                  | 500                        | 550                       | $3.67 \pm 1.83$                 | $5.19 \pm 2.37$                   |
| MDJS98      |               | 760                       | $610 \pm 80$                   | $1.68 \pm .62$                  | 680                        | 750                       | $5.00 \pm 2.50$                 | $6.68 \pm 3.12$                   |
| <b>MEAN</b> |               | <b>~670</b>               | <b><math>540 \pm 70</math></b> | <b><math>1.5 \pm 0.5</math></b> | <b>527</b>                 | <b>580</b>                | <b><math>3.9 \pm 1.9</math></b> | <b><math>5.35 \pm 2.47</math></b> |
| MDJS23b     | <b>PS2</b>    | 410                       | $330 \pm 40$                   | $0.91 \pm 0.33$                 | 670                        | 740                       | $4.93 \pm 2.46$                 | $5.84 \pm 2.79$                   |
| MDJS96      |               | 400                       | $320 \pm 40$                   | $0.88 \pm 0.32$                 | 700                        | 770                       | $5.13 \pm 2.56$                 | $6.01 \pm 2.88$                   |
| MDJS97      |               | 430                       | $345 \pm 45$                   | $0.95 \pm 0.35$                 | 580                        | 640                       | $4.26 \pm 2.13$                 | $5.21 \pm 2.48$                   |
| <b>MEAN</b> |               | <b>~415</b>               | <b><math>330 \pm 40</math></b> | <b><math>0.9 \pm 0.3</math></b> | <b>650</b>                 | <b>720</b>                | <b><math>4.8 \pm 2.4</math></b> | <b><math>5.69 \pm 2.72</math></b> |

Bold lines display the mean values found for each perched basin.

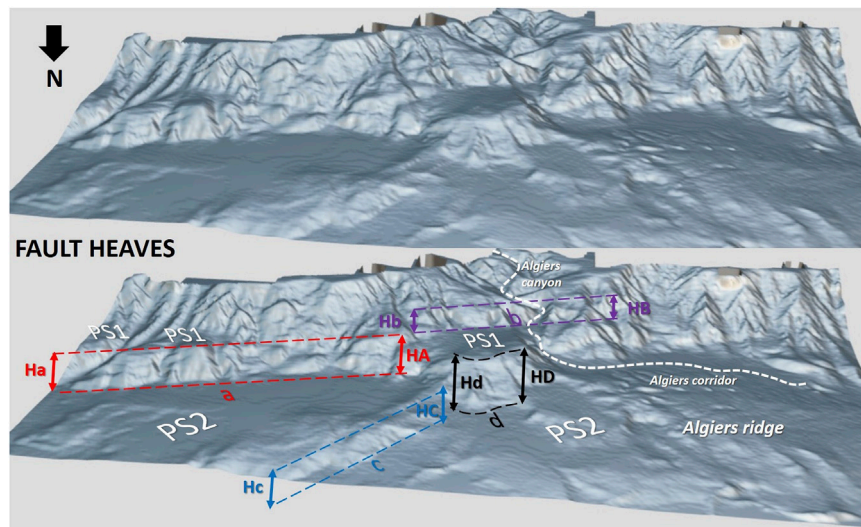


**FIGURE 10** Perspective view towards the south of the boumerdès slope and basin in a “MatCap” geometry plot (<https://sketchfab.com/3d-models/marge-boumerdes-e160112567d745bdb5e80d9f7dd1a64c>) displaying the main cumulative scarps identified off Boumerdès. Bottom figure provides our interpretation of fault heaves Ha-HA and Hb-HB for Fault F1 (Fe1 and Fo1, respectively), and Hc-HC and Hd-HD for Fault F2 (Fe2 and Fo2, respectively). PS1 and PS2 refer to the perched surfaces mapped on Figure 2. Assumed faults F1 and F2 are shown on Figure 7; Figure 11. Measured values are reported in Table 2.

the top of fault ramps identified at mid-slope and in the lower slope (see e.g. Déverchère et al., 2005; Domzig et al., 2006; Strzeczynski et al., 2010; Capron et al., 2011), and 2) their length and geometrical position mimic the length, strike and upward prolongation of the main rupture of the 2003 Boumerdès earthquake, provided that a northward shift is caused by two flats in the fault geometry (see §4.3). Here, we try to show how much these anomalies can be

followed along strike in order to estimate average fault heaves. The “dives” made thanks to VR (SM1) allow us to propose four main scarps that are consistently followed in the morphology, either as linear scarps or curved ones (Figure 10; Table 2):

- Scarp a) is the longest one and extends over ~40 km from the Isser canyon to Dellys canyon (Figure 3; Cattaneo et al.,

**TABLE 2** Characteristics of the main cumulative scarps identified off Boumerdès. Scarps, perched surfaces and heaves are identified on [Figure 10](#). Heave values represent only the vertical components.

| Scarp | Length (km) | Place on scarp | Depth bsl (m) |       | Height (m) |      | Scarp heave (m) | Upper surface | Lower surface | Assumed fault |
|-------|-------------|----------------|---------------|-------|------------|------|-----------------|---------------|---------------|---------------|
|       |             |                | West          | East  | West       | East |                 |               |               |               |
| a     | 41          | Top            | 1650          | 1542  | 744        | 793  | 769 ± 25        | PS1           | PS2           | Fe1           |
|       |             | Base           | 2,394         | 2,335 |            |      |                 |               |               |               |
| b     | 27          | Top            | 735           | 765   | 284        | 339  | 312 ± 28        | Upper slope   | PS1           | Fo1           |
|       |             | Base           | 1019          | 1104  |            |      |                 |               |               |               |
| c     | 30          | Top            | 2,317         | 2,401 | 307        | 315  | 311 ± 4         | PS2           | Deeper basin  | Fe2           |
|       |             | Base           | 2,624         | 2,716 |            |      |                 |               |               |               |
| d     | 18          | Top            | 1499          | 1644  | 776        | 866  | 821 ± 45        | PS1           | PS2           | Fo2           |
|       |             | Base           | 2,275         | 2,510 |            |      |                 |               |               |               |

2010). It is about 770 m high and has approximately the same length, strike and longitudinal position as the eastern patch of the 2003 Boumerdès slip model ([Figure 2](#)). Its base coincides with the thrust fault segment Fe1 ([Figure 7](#); [Déverchère et al., 2005](#); [Strzeczynski et al., 2021](#)).

- Scarp b) is in the western prolongation of Scarp a) but is shifted upward on the slope and can be followed on both sides of the Algiers canyon along ~27 km with a mean height of 312 m. It corresponds quite well in length, strike and longitudinal position to the western patch of the 2003 Boumerdès slip model ([Figure 2](#)). Its base coincides with the thrust fault segment Fo1 ([Figure 7](#); [Déverchère et al., 2005](#); [Strzeczynski et al., 2021](#)).
- Scarp c) marks the outward limit of the large PS2 surface. It is relatively similar to Scarp b) in length (~30 km) and height (about 310 m) but is far inside the basin and slightly oblique to the margin. It largely overlaps Scarp a).
- Finally, Scarp d) makes a curved step ~18 km long around the circular PS1 surface. It is the highest scarp (~820 m) we have identified. It partly overlaps Scarp b) on its eastern side and is limited to the west by the Algiers canyon.

Note that the cumulative heaves across strike are rather similar from east (a and c: ~1080 m) to west (b and d: ~1130 m).

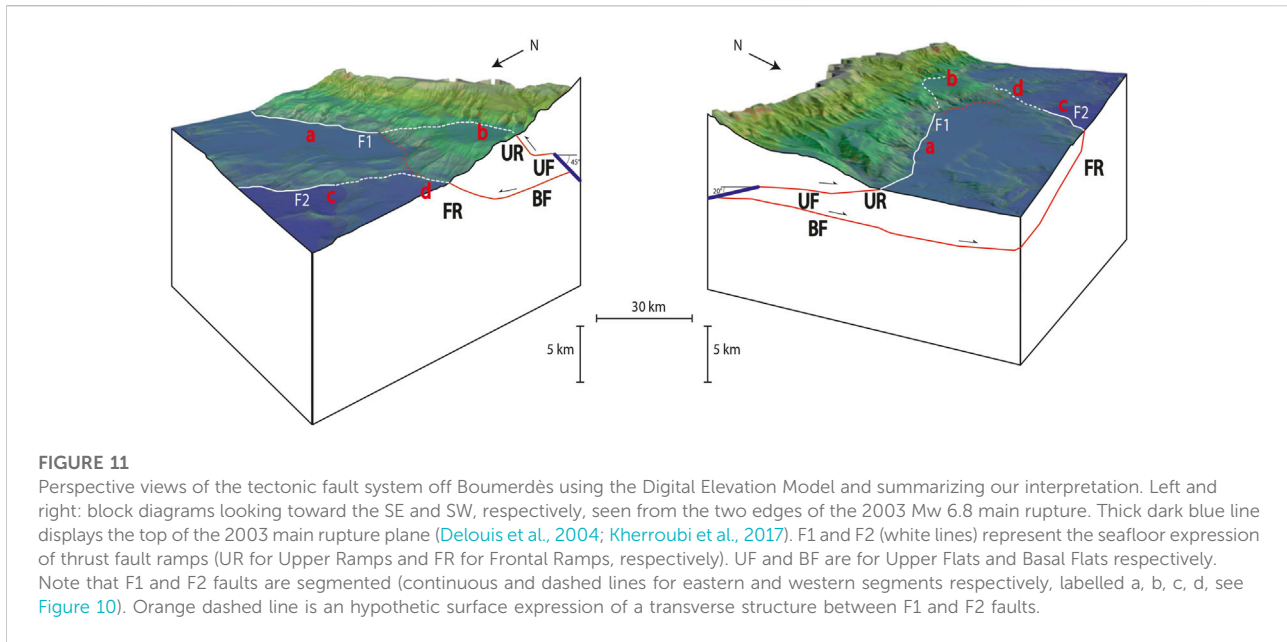
## 5 Discussion

### 5.1 Relationships between the 2003 coseismic rupture zone and geomorphic signatures

The morphometric analysis of the submarine canyons and interflaves of the central Algerian margin off Boumerdès has revealed deeply incised and very active canyons, as found also in

the western margin of Algeria ([Amir and Theilen-Willige, 2022](#); [Fernane et al., 2022](#)), thus evidencing the importance of turbidity currents and gravity slides in shaping the sea floor ([Dan et al., 2009](#); 2010; [Cattaneo et al., 2010](#)). However, canyons off the Boumerdès coast appear to be generally less ramified and with a general tendency to a moderate concavity, supporting a relatively higher maturity than canyons off western Algeria. Above all, the longitudinal profiles inside and outside thalwegs of canyons and gullies have recorded morphometric anomalies (“knickpoint zones”) of several kilometers width and several hundred meters amplitude ([Figure 4](#); [Figure 6](#)). These large knickpoints are systematically observed between Boumerdès and Dellys cities, where the 2003 May 21 rupture zone is located, but disappear on the westernmost segment of the slope striking almost W-E and located outside the main rupture area of the 2003 Boumerdès earthquake, off the bay of Algiers ([Figures 3–6](#)), at a place where a coseismic segment striking N100° and displaying much smaller slip values is identified ([Ouyed et al., 2011](#); [Beldjoudi and Delouis, 2022](#)). These slope breaks are located either at mid-slope (west) or at the margin toe (west and east), supporting that they result from repeated slips on active thrust faults (F1 on the slope, F2 in the deep basin; [Figure 7](#)). While canyon profiles have hardly preserved the tectonic imprints of Fault F1 ([Figure 4](#); [Figure 10](#)), scarps appear quite well preserved in interflaves ([Figure 6](#); [Figure 10](#)). This result strongly suggests that the rate of erosion within the active canyons of the slope is of the same order of magnitude as the slip rates, at least on F1 Fault.

The fact that the perched surfaces PS1 and basins (PB1) provide similar geometries and ages along the whole sector of the margin support the hypothesis that the fault ramps responsible for their formation belong to the same fault system initiated about 1.5 Myr ago ([Table 1](#)). Furthermore, the quite good agreement in length, strike and longitudinal position between scarps a (fault Fe1) and b (fault Fo1) and the two main rupture patches of the 2003 Boumerdès slip model ([Delouis et al., 2004](#);



Belabbès et al., 2009; Beldjoudi and Delouis, 2022) supports that they correspond to the cumulative surface expression of the Boumerdès fault at depth. Therefore, we suggest that scarps a and b (Figure 10) represent two segments of different dips of the same fault system that ruptured along its whole length on 21 May 2003.

## 5.2 Implications on fault geometry and strain rates

The careful examination of the geomorphology of the continental margin in the area between Algiers and Dellys has allowed us to isolate four main morphological scarps of several hundred meters high correlated along strike over several tens of kilometers distance (Figure 10; Table 2). We have interpreted them as Quaternary cumulative fault scarps linked to the activity of two thrust ramps sub-parallel to the margin and dipping southward. No significant cumulative deformation expressed as scarps or depocenters is found in the uppermost slope or in the narrow continental shelf, ruling out the hypothesis that the active thrust responsible for the 2003 Mw 6.8 earthquake remains with a constant dip up to the seafloor (Ayadi et al., 2008; 2010; Belabbès et al., 2009). Instead, our analysis supports that a ramp-on-flat geometry of the main thrust enhances the birth of slope breaks shifted northward relative to the rupture zone (Déverchère et al., 2005; 2010; Strzeczynski et al., 2010; 2021; Kherroubi et al., 2017). The spatial distribution of fault scarps (Figures 10,11) evidences a major lateral change in the fault geometry towards the surface: to the west, from the western tip of the 2003 main rupture zone to the epicenter (Figure 2), the

morphological scarps are located on the slope b) and at the margin toe d), while to the east, from the epicenter to Dellys city (Figure 2), they are located at the margin toe a) and ~20 km in the deep domain c). Such along-strike complexities of thrust systems are commonly reported in fold-and-thrust belts. They may result from a geometric barrier associated with the progressive transfer of rupture between fault segments with different planes, as suggested by King and Yielding (1984) for the El Asnam thrust fault system which ruptured in 1980 with a magnitude 7.3 earthquake in western Algeria. We suggest that the along-strike segmentation we observe off Boumerdès may result from a similar process of thrust fault evolution through time: a geometrical barrier may explain the existence of two patches in the coseismic slip distribution, but also a partitioning of strain across strike on two fault ramps with various dip angles (Delouis et al., 2004; Kherroubi et al., 2017). Figure 11 summarizes in a 3D perspective view our interpretation of the link between the main 2003 rupture segments at depth and the assumed basal and shallow flats and ramps towards the surface. This pattern of lateral variation of the inverted structures and of outward thrust propagation is well modeled in analog and numerical experiments where successive thick-skinned thrusts drive thin-skinned detachments (Pfiffner, 2017; Granado and Ruh, 2019; Strzeczynski et al., 2021). The significantly younger age of PB2 relative to PB1 (Table 1) supports this hypothesis of frontal fault propagation, although both fault ramps are apparently still active today (Figures 8, 9). We have also found that the sum of vertical fault heaves across strike (Figure 10; Table 2) do not differ significantly from west to east and is of the order of 1100 m, suggesting that long-term slip rates are similar along strike. If we consider the mean heave

**TABLE 3** Hypothetical horizontal strain rates across the two segments of the Boumerdès margin using assumed heaves on the four main scarps and ages of growth strata in perched basins PS1 and PS2. Age of onset for Scarp b is unknown and has been assumed as equivalent to the one of Scarp d. See text for details.

| Fault segment | Assumed fault dip | Scarp | Mean vertical offset (m) | Horizontal displacement (m) | Age of onset | Horizontal strain rate/scarp | Horizontal strain rate/segment |
|---------------|-------------------|-------|--------------------------|-----------------------------|--------------|------------------------------|--------------------------------|
| Western       | 40°               | Hb-HB | 312                      | 371                         | 1.5 Ma?      | 0.25 mm/yr                   | 0.9 mm/yr                      |
|               |                   | Hd-HD | 821                      | 978                         | 1.5 Ma       | 0.65 mm/yr                   |                                |
| Eastern       | 20°               | Ha-HA | 769                      | 2,113                       | 1.5 Ma       | 1.41 mm/yr                   | 2.3 mm/yr                      |
|               |                   | Hc-HC | 311                      | 854                         | 0.9 Ma       | 0.95 mm/yr                   |                                |

values to be representative of the long term deformation of the margin, we may use the mean ages found for the onsets of PB1 and PB2 growth strata (S4.3) to estimate horizontal slip rates on the four blind thrust ramps (Table 3). In the absence of accurate measurements of fault dips, we use the two average dips deduced from rupture modeling and aftershock distribution from the 2003 Boumerdès earthquake, i.e.  $\sim 40^\circ$  and  $\sim 20^\circ$  for the western and eastern segments respectively (Delouis et al., 2004; Kherroubi et al., 2017). Age and dip uncertainties are high, therefore we consider that the average values computed here are only indicative and provide a way to bracket values of horizontal strain rates. We find that horizontal shortening rates likely range between .9 and 2.3 mm/yr across the central Algerian margin (Table 3). The mean value of 1.6 mm/yr is quite close to the horizontal shortening rate of about 1.5 mm/yr proposed by Bougrine et al. (2019) in the offshore domain at the longitude of Boumerdès from geodetic measurements. Furthermore, the tectonic uplift rate inferred from the scarps F1 and F2 identified in our study (Figure 7; Figure 11, i.e.  $\sim 7$  mm/yr (about 1100 m within  $\sim 1.5$  Ma), is of the same order of magnitude than the long-term coastal uplift rates assessed in the region of Algiers ( $\sim 5$  mm/yr, see Raymond, 1976; Authemayou et al., 2017; Strzeczynski et al., 2021). Therefore, the cumulative strain rates deduced from the two thrust systems (F1 and F2) off Boumerdès are in agreement with present-day predictions of shortening rates in the offshore domain between the Balearic and Algerian coasts, suggesting that these two blind thrust ramps accommodate most of the plate convergence in the offshore domain at this longitude since Quaternary times.

## 6 Concluding remarks

The submarine slope west of Algiers City has undergone a major earthquake in 2003 that had dramatic consequences along the coastline between Algiers and Dellys cities and triggered numerous turbidity currents on the slope and cable breaks in the deep basin. Thanks to the use of new tools developed in VR combined with classical GIS methods, we were able to closely link the main geomorphological features of the continental slope and deep basin

(especially slope breaks) with the Plio-Quaternary sediments trapped on the slope and at the margin toe. Our analysis reveals four main slope breaks and two perched surfaces corresponding to Quaternary growth strata tilted towards the continent. Although the scarps and basins appear to be deeply incised by numerous canyons and gullies, they can be followed and correlated over several tens of kilometers along strike. The cumulative scarps located southward are controlling the tilting of the narrow basin upslope and are interpreted as south-dipping thrust ramps matching the 2003 coseismic rupture zone in length, strike, longitudinal position and segmentation. We do not report any inversion of previous normal faults of the passive margin, as often found in inversion of rift basins, but basement faulting of opposite vergence in a thick-skinned tectonic style. The total vertical throw of the overlapping scarps exceeds 1000 m high, supporting a significant uplift of the hanging wall of the Algerian margin during Quaternary times. Our results support northward frontal propagation of an active thrust system by two main ramp-on-flat intra-crustal detachment levels classically found during basin inversions or in fold-and-thrust belts. We estimate Quaternary shortening rates of about 1.5 mm/yr on these two fault systems, a value that is representative of geodetic strain rates across the western Mediterranean basin. The tectonic model we propose (Figure 11) remains a simplified sketch which does not rule out the existence of other active secondary faults (Ouyed et al., 2011; Beldjoudi and Delouis, 2022).

The VR tools developed for the purpose of this study provide new possibilities for research and training, especially when the fault system displays three-dimensional geometrical complexities. However, they are not yet interactive enough in the sense that the user cannot measure or annotate in VR: this requires new developments to allow back and forth between the traditional GIS interface and the VR environment. We also hope to integrate various dynamic simulations (fault kinematics, turbidity currents, submarine slides) to evaluate how the morphology evolves in relation to these processes.

## Data availability statement

The data analyzed in this study is subject to the following licenses/restrictions: Bathymetric and seismic data used in this



study were obtained during the 2003 MARADJA (doi: 10.17600/5020080) and the 2005 MARADJA2 (doi: 10.17600/5020080) and SAMRA (doi: 10.17600/5020090) experiments on board of the Research Vessel “Le Suroît” and are subject to a formal agreement between Algeria and France. The data are stored and managed by SISMER (Ifremer) and are submitted to restricted access. Requests to access these datasets should be directed to [Cecile.Pertuisot@ifremer.fr](mailto:Cecile.Pertuisot@ifremer.fr).

## Author contributions

JD wrote the original draft of this manuscript, designed the tasks and supervised them. AB organized the database, realized the GIS analysis and figures, and contributed to the Virtual Reality exploration. MK undertook the Virtual Reality environment and developed the tools used in this study. MJ supervised the GIS analysis and the Virtual Reality exploration. RR designed the pedagogical approach of the Virtual Reality and criticized all stages of the project. All authors contributed to manuscript reading and approved the submitted version.

## Funding

This research was provided by a grant from the French government under the program “Investissements d’Avenir” which has created the Ecole Universitaire de Recherche (EUR) ISblue, interdisciplinary graduate school for the blue planet (ANR-17-EURE-0015).

## Acknowledgments

This work is part of the ISblue AISMERALDA (*Ateliers Immersifs Sous-Marins et Réalité Augmentée: Littoral, Dorsales, Autres*) project aiming at building pedagogical

## References

- Abbassene, F., Chazot, G., Bellon, H., Bruguier, O., Ouabadi, A., Maury, R. C., et al. (2016). A 17 Ma onset for the post-collisional K-rich calc-alkaline magmatism in the Maghrebides: Evidence from Bougaroun (northeastern Algeria) and geodynamic implications. *Tectonophysics* 674, 114–134. doi:10.1016/j.tecto.2016.02.013
- Amir, L., and Theilen-Willige, B. (2022). Coastal environmental impact of geohazards in the area of the habibas islands (western Algeria, alboran): Insights from GIS-analysis and remote sensing. *Eur. J. Environ. Earth Sci.* 3 (4), 48–58. doi:10.24018/ejgeo.2022.3.4.303
- Authemayou, C., Pedoja, K., Heddar, A., Molliex, S., Boudiaf, A., Ghaleb, B., et al. (2017). Coastal uplift west of Algiers (Algeria): Pre- and post-Messinian sequences of marine terraces and rasas and their associated drainage pattern. *Int. J. Earth Sci.* 106, 19–41. doi:10.1007/s00531-016-1292-5
- Auzemery, A., Willingshofer, E., Sokoutis, D., Brun, J. P., and Cloetingh, S. A. P. L. (2021). Passive margin inversion controlled by stability of the mantle lithosphere. *Tectonophysics* 817, 229042. doi:10.1016/j.tecto.2021.229042

scenarios for MsC students by using multisource data sets in selected marine and coastal virtual environments. We are indebted to Karim Yelles (*Centre de Recherches en Astronomie, Astrophysique et Géophysique*, Algiers, Algeria), Rabah Bracene (Sonatrach, Boumerdès, Algeria) and all the scientists involved in the Algerian-French cruises MARADJA (2003) and MARADJA2/SAMRA (2005). We are grateful to Antonio Cattaneo (Ifremer, France), Bernard Mercier de Lépinay (CNRS, UCA, Nice, France), Nathalie Babonneau, David Graindorge (UBO University, France), Stéphane Dominguez (Montpellier University, France), Anne Domzig (Petronas, Kuala Lumpur, Indonesia) and Pierre Strzeczynski (Le Mans University, France) for methodological support at different stages of this work and for fruitful discussions.

## Conflict of interest

The authors declare that the research was conducted in the absence of any commercial or financial relationships that could be construed as a potential conflict of interest.

## Publisher’s note

All claims expressed in this article are solely those of the authors and do not necessarily represent those of their affiliated organizations, or those of the publisher, the editors and the reviewers. Any product that may be evaluated in this article, or claim that may be made by its manufacturer, is not guaranteed or endorsed by the publisher.

## Supplementary material

The Supplementary Material for this article can be found online at: <https://www.frontiersin.org/articles/10.3389/feart.2022.1010226/full#supplementary-material>

- Ayadi, A., Dorbath, C., Ousadou, F., Maouche, S., Chikh, M., Bounif, M. A., et al. (2010). Reply to comment by J. Déverchère et al. on “Zemmouri earthquake rupture zone ( $M_w$ 6.8, Algeria): Aftershocks sequence relocation and 3D velocity model”. *J. Geophys. Res.* 115 (B4), B04319. doi:10.1029/2009JB006705

- Ayadi, A., Dorbath, C., Ousadou, F., Maouche, S., Chikh, M., Bounif, M. A., et al. (2008). Zemmouri earthquake rupture zone ( $M_w$ 6.8, Algeria): Aftershocks sequence relocation and 3D velocity model. *J. Geophys. Res.* 113 (9), B09301. doi:10.1029/2007JB005257

- Ayadi, A., Maouche, S., Harbi, A., Meghraoui, M., Beldjoudi, H., Oussadou, F., et al. (2003). Strong Algerian earthquake strikes near capital city. *Eos Am. Geophys. Union.* 84, 561. doi:10.1029/2003EO500002

- Babonneau, N., Cattaneo, A., Ratzov, G., Déverchère, J., Yelles-Chaouche, A., Lateb, T., et al. (2017). Turbidite chronostratigraphy off Algiers, central Algerian margin: A key for reconstructing holocene paleo-earthquake cycles. *Mar. Geol.* 384, 63–80. doi:10.1016/j.margeo.2016.10.017

- Babonneau, N., Cattaneo, A., Savoye, B., Barjavel, G., Déverchère, J., and Yelles, K. (2012). "The kramis deep-sea fan off Western Algeria: Role of sediment waves in turbiditic levee growth," in *Application of the principles of seismic geomorphology to continental-slope and base-of-slope systems: Case studies from seafloor and near-seafloor analogues*. Editors B. E. Prather, M. E. Deptuck, D. Mohrig, B. Van Hoorn, and R. B. Wynn (Broken Arrow, Tulsa: SEPM Special Publication), 99. (ISBN: 978-1-56576-304-3). doi:10.2110/pec.12.99
- Belabbès, S., Wicks, C., Kahir, Z., and Meghraoui, M. (2009). Rupture parameters of the 2003 Zemmouri earthquake ( $M_w$ 6.8), Algeria, earthquake from joint inversion of interferometric synthetic aperture radar, coastal uplift, and GPS. *J. Geophys. Res.* 114, B03406. doi:10.1029/2008JB005912
- Beldjoudi, H., and Delouis, B. (2022). Reassessing the rupture process of the 2003 Boumerdes-Zemmouri earthquake (Mw 6.8, northern Algeria) using teleseismic, strong motion, InSAR, GPS, and coastal uplift data. *Mediterr. Geosci. Rev.* 53. doi:10.1007/s42990-022-00090-z
- Bellalem, F., Talbi, A., and Maouche, S. (2022). A unified MW parametric earthquake catalog for Algeria and adjacent regions (PECAAR). *Med. Geosci. Rev.* doi:10.1007/s42990-022-00085-w
- Billant, J., Bozzio, J., Leclerc, F., Escartin, J., Gracias, N., Istenic, K., et al. (2019). "Performing submarine field survey without scuba gear using GIS-like mapping in a Virtual Reality environment," in *OCEANS 2019-Marseille* (IEEE), 1–6. doi:10.1109/OCEANS.2019.8867408
- Billi, A., Cuffaro, M., Orecchio, B., Palano, M., Presti, D., and Totaro, C. (2023). Retracing the Africa–Eurasia nascent convergent boundary in the Western Mediterranean based on earthquake and GNSS data. *Earth Planet. Sci. Lett.* 601, 117906. doi:10.1016/j.epsl.2022.117906
- Blondel, S., Bellucci, M., Evans, S., Del Ben, A., and Camerlenghi, A. (2022). Contractional salt deformation in a recently inverted basin: Miocene to current salt deformation within the central Algerian basin. *Basin Res.* 00, 1632–1654. doi:10.1111/bre.12673
- Bonali, F. L., Russo, E., Vitello, F., Antoniou, V., Marchese, F., Fallati, L., et al. (2022). How academics and the public experienced Immersive Virtual Reality for geo-education. *Geosciences* 12, 9. doi:10.3390/geosciences12010009
- Bougrine, A., Yelles-Chaouche, A. K., and Calais, E. (2019). Active deformation in Algeria from continuous GPS measurements. *Geophys. J. Int.* 217 (1), 572–588. doi:10.1093/gji/ggz035
- Boullin, J. P. (1986). Le bassin maghrébin, une ancienne limite entre l'Europe et l'Afrique à l'ouest des Alpes. *Bull. Société Géologique Fr.* II (4), 547–558. doi:10.2113/gssgfbull.II.4.547
- Camerlenghi, A., Accettella, D., Costa, S., Lastras, G., Acosta, J., Canals, M., et al. (2009). Morphogenesis of the SW Balearic continental slope and adjacent abyssal plain, Western Mediterranean Sea. *Int. J. Earth Sci.* 98, 735–750. doi:10.1007/s00531-008-0354-8
- Capron, A., Déverchère, J., Gaullier, V., Le Roy, P., Mercier de Lépinay, B., and Yelles, K. (2011). "Algerian margin," in *Seismic atlas of the Messinian salinity crisis markers in the offshore Mediterranean domain*, Co-Ed. Editors J. Lofi and J. Déverchère. (Paris, France: Mémoire de la Société géologique de France and Commission for the Geological Map of the World), 179, 72. ISBN 2-85363-097-8.
- Cattaneo, A., Babonneau, N., Dan, G., Déverchère, J., Domzig, A., Gaullier, V., et al. (2010). Submarine landslides along the Algerian margin: A review of their occurrence and potential link with tectonic structures. *Submar. mass movements their consequences*, 515–525. doi:10.1007/978-90-481-3071-9\_42
- Chazot, G., Abbassene, F., Maury, R. C., Déverchère, J., Bellon, H., Ouabadi, A., et al. (2017). An overview on the origin of post-collisional miocene magmatism in the kabylies (northern Algeria): Evidence for crustal stacking, delamination and slab detachment. *J. Afr. Earth Sci.* 125, 27–41. doi:10.1016/j.jafrearsci.2016.10.005
- Cope, M. J. (2003). Algerian licensing round may offer opportunity for exploration plays in deep offshore frontier. *First Break* 21, 37–42. doi:10.3997/1365-2397.21.7.25550
- Covault, J. A., Fildani, A., Romans, B. W., and McHargue, T. (2011). The natural range of submarine canyon-and-channel longitudinal profiles. *Geosphere* 7 (2), 313–332. doi:10.1130/GES00610.1
- Dal Cin, M., Del Ben, A., Mocnik, A., Accaino, F., Geletti, R., Wardell, N., et al. (2016). Seismic imaging of late miocene (messinian) evaporites from western mediterranean back-arc basins. *Pet. Geosci.* 22, 297–308. doi:10.1144/ptgeo2015-096
- Dan, G., Sultan, N., Cattaneo, A., Déverchère, J., Yelles, K., and Mosher, D. C. (2010). "Mass-transport deposits on the Algerian margin (Algiers area): Morphology, lithology and sedimentary processes advances in natural and technological hazards research," in *Submarine mass movements and their consequences*. Editors C. Ship, L. Moscardelli, J. Chaytor, C. Baxter, H. Lee, and R. Urgeles, 28, 527–539. doi:10.1007/978-90-481-3071-9\_43
- Dan, G., Sultan, N., Savoye, B., Déverchère, J., and Yelles, K. (2009). Quantifying the role of sandy-silty sediments in generating slope failures during earthquakes: Example from the Algerian margin. *Int. J. Earth Sci. Rundsch* 98 (4), 769–789. doi:10.1007/s00531-008-0373-5
- Delouis, B., Vallée, M., Meghraoui, M., Calais, E., Maouche, S., Lammali, K., et al. (2004). Slip distribution of the 2003 Boumerdes-Zemmouri earthquake, Algeria, from teleseismic, GPS, and coastal uplift data. *Geophys. Res. Lett.* 31 (18), L18607. doi:10.1029/2004GL020687
- Déverchère, J., de Lépinay, B. M., Cattaneo, A., Strzeczynski, P., Calais, E., Domzig, A., et al. (2010). Comment on "Zemmouri earthquake rupture zone ( $M_w$ 6.8, Algeria): Aftershocks sequence relocation and 3D velocity model" by A. Ayadi et al. *J. Geophys. Research-solid Earth* 115 (B04320), B04320–B04326. doi:10.1029/2008JB006190
- Déverchère, J., Yelles, K., Domzig, A., Mercier de Lépinay, B., Boullin, J. P., Gaullier, V., et al. (2005). Active thrust faulting offshore Boumerdes, Algeria, and its relations to the 2003 Mw 6.9 earthquake. *Geophys. Res. Lett.* 32 (4). doi:10.1029/2004GL021646
- Do Couto, D., Popescu, S. M., Suc, J.-P., Melinte-Dobrinescu, M. C., Barhoun, N., Gorini, C., et al. (2014). Lago mare and the messinian salinity crisis: Evidence from the Alboran sea (S. Spain). *Mar. Petroleum Geol.* 52, 57–76. doi:10.1016/j.marpetgeo.2014.01.018
- Domzig, A., Yelles, K., Le Roy, C., Déverchère, J., Boullin, J. P., Bracène, R., et al. (2006). Searching for the Africa–Eurasia Miocene boundary offshore Western Algeria (MARADJA'03 cruise). *Comptes Rendus Geosci.* 338 (1–2), 80–91. doi:10.1016/j.crte.2005.11.009
- Ercilla, G., Galindo-Zaldívar, J., Estrada, F., Valencia, J., Juan, C., Casas, D., et al. (2022). Understanding the complex geomorphology of a deep sea area affected by continental tectonic indentation: The case of the Gulf of Vera (Western Mediterranean). *Geomorphology* 402, 108126. doi:10.1016/j.geomorph.2022.108126
- Fernane, L., Matougui, R., Amarni, N., and Belkessa, R. (2022). Variation in canyon morphology and their relationship with tectonic: The example of the Western Algerian margin. *Arabian J. Geosciences* 15, 254. doi:10.1007/s12517-022-09566-6
- Giresse, P., Pauc, H., Déverchère, J., and Party, M. S. S. (2009). Sedimentary processes and origin of sediment gravity-flow deposits on the Western Algerian margin during late Pleistocene and Holocene. *Mar. Petroleum Geol.* 26 (5), 695–710. doi:10.1016/j.marpetgeo.2008.03.011
- Graindorge, D., Klingelhoefer, F., Sibuet, J. C., McNeill, L., Henstock, T. J., Dean, S., et al. (2008). Impact of lower plate structure on upper plate deformation at the NW Sumatran convergent margin from seafloor morphology. *Earth Planet. Sci. Lett.* 275 (3–4), 201–210. doi:10.1016/j.epsl.2008.04.053
- Granado, P., and Ruh, J. B. (2019). Numerical modelling of inversion tectonics in fold-and-thrust belts. *Tectonophysics* 763, 14–29. doi:10.1016/j.tecto.2019.04.033
- Gutscher, M. A., Kopp, H., Krastel, S., Bohrmann, G., Garlan, T., Zaragosi, S., et al. (2017). Active tectonics of the Calabrian subduction revealed by new multi-bathymetric data and high-resolution seismic profiles in the Ionian Sea (Central Mediterranean). *Earth Planet. Sci. Lett.* 461, 61–72. doi:10.1016/j.epsl.2016.12.020
- Haidar, S., Déverchère, J., Graindorge, D., Arab, M., Medaouri, M., and Klingelhoefer, F. (2022). Back-arc dynamics controlled by slab rollback and tearing: A reappraisal of seafloor spreading and kinematic evolution of the eastern Algero-Balearic basin (Western mediterranean) in the middle-late miocene. *Tectonics* 41, e2021TC006877. doi:10.1029/2021TC006877
- Hamai, L., Petit, C., Abtout, A., Yelles-Chaouche, A., and Déverchère, J. (2015). Flexural behaviour of the north Algerian margin and tectonic implications. *Geophys. J. Int.* 201, 1426–1436. doi:10.1093/gji/ggv098
- Hamdache, M., Peláez, J. A., Talbi, A., and Casado, C. L. (2010). A unified catalog of main earthquakes for Northern Algeria from AD 856 to 2008. *Seismol. Res. Lett.* 81 (5), 732–739. doi:10.1785/gssrl.81.5.732
- Heezen, B. C., and Ewing, M. (1955). Orleansville earthquake and turbidity currents. *Am. Assoc. Petroleum Geol. Bull.* 39, 2505–2514.
- Hsü, K. J., Cita, M. B., and Ryan, W. B. F. (1973). The origin of the Mediterranean evaporites, Initial Reports of the Deep Sea Drilling Project. Washington, DC: U.S. Government Printing Office, 43, 1203–1231.
- Jaud, M., Geoffroy, L., Chauvet, F., Durand, E., and Civet, F. (2022). Potential of a virtual reality environment based on very-high-resolution satellite imagery for structural geology measurements of lava flows. *J. Struct. Geol.* 158, 104569. doi:10.1016/j.jsg.2022.104569
- Kherroubi, A., Déverchère, J., Yelles, K., Mercier de Lépinay, B., Domzig, A., Cattaneo, A., et al. (2009). Recent and active deformation pattern off the easternmost Algerian margin, Western Mediterranean Sea: New evidence for contractional tectonic reactivation. *Mar. Geol.* 261 (1–4), 17–32. doi:10.1016/j.margeo.2008.05.016

- Kherroubi, A., Yelles-Chaouche, A., Koulakov, I., Déverchère, J., Beldjoudi, H., Haneed, A., et al. (2017). Full aftershock sequence of the M w 6.9 2003 boumerdes earthquake, Algeria: Space-time distribution, local tomography and seismotectonic implications. *Pure Appl. Geophys.* 174 (7), 2495–2521. doi:10.1007/s00024-017-1571-5
- King, G., and Yielding, G. (1984). The evolution of a thrust fault system: Processes of rupture initiation, propagation and termination in the 1980 El Asnam (Algeria) earthquake. *Geophys. J. R. Astronomical Soc.* 77, 915–933. doi:10.1111/j.1365-246X.1984.tb02229.x
- Leclaire, L. (1970). *Plateau continental nord-africain: Nature de la couverture sédimentaire actuelle et récente*. Thèse d'Etat. Paris, France: Université de Paris, 391.
- Leffondré, P., Déverchère, J., Medaouri, M., Klingelhofer, F., Graindorge, D., and Arab, M. (2021). Ongoing inversion of a passive margin: Spatial variability of strain markers along the Algerian margin and basin (Mediterranean Sea) and seismotectonic implications. *Front. Earth Sci.* 9, 674584. doi:10.3389/feart.2021.674584
- Leprêtre, R., Frizon de Lamotte, D., de Combier, V., Gimeno-Vives, O., Mohn, G., and Eschard, R. (2018). The Tell-Rif orogenic system (Morocco, Algeria, Tunisia) and the structural heritage of the southern Tethys margin. *BSGF - Earth Sci. Bull.* 189 (2), 10. doi:10.1051/bsgf/2018009
- Lofi, J., Sage, F., Déverchère, J., Loncke, L., Maillard, A., Gaullier, V., et al. (2011). Refining our knowledge of the Messinian salinity crisis records in the offshore domain through multi-site seismic analysis. *Bull. Soc. Geol. Fr.* 182, 163–180. doi:10.2113/gssgfbull.182.2.163
- Mahsas, A., Lammali, K., Yelles, K., Calais, E., Freed, A. M., and Briole, P. (2008). Shallow afterslip following the 2003 may 21, Mw = 6.9 boumerdes earthquake, Algeria. *Geophys. J. Int.* 172, 155–166. doi:10.1111/j.1365-246X.2007.03594.x
- Maillard, A., and Mauffret, A. (2013). Structure and present-day compression in the offshore area between alicante and ibiza island (eastern iberian margin). *Tectonophysics* 591, 116–130. doi:10.1016/j.tecto.2011.07.007
- Martinez-Garcia, P., Comas, M., Soto, J. I., Lonergan, L., and Watts, A. B. (2013). Strike-slip tectonics and basin inversion in the western mediterranean: The post-messinian evolution of the Alboran sea. *Basin Res.* 25, 361–387. doi:10.1111/bre.12005
- Meghraoui, M., Maouche, S., Chemaa, B., Cakir, Z., Aoudia, A., Harbi, A., et al. (2004). Coastal uplift and thrust faulting associated with the Mw= 6.8 Zemmouri (Algeria) earthquake of 21 May, 2003. *Geophys. Res. Lett.* 31, L19605. doi:10.1029/2004gl020466
- Menard, H. W. (1955). Deep-sea channels, topography, and sedimentation. *Am. Assoc. Petroleum Geol. Bull.* 39, 236–255.
- Métois, M., Martelat, J. E., Billant, J., Andreani, M., Escartín, J., et al. (2021). Deep oceanic submarine fieldwork with undergraduate students: An immersive experience with the minerve software. *Solid earth.* 12 (12), 2789–2802. doi:10.5194/se-12-2789-2021
- Mitchell, N. C. (2005). Interpreting long-profiles of canyons in the USA Atlantic continental slope. *Mar. Geol.* 214, 75–99. doi:10.1016/j.margeo.2004.09.005
- Morgan, J. K., Solomon, E. A., Fagereng, A., Savage, H. A., Wang, M., Meneghini, F., et al. (2022). Seafloor overthrusting causes ductile fault deformation and fault sealing along the Northern Hikurangi Margin. *Earth Planet. Sci. Lett.* 593, 117651. doi:10.1016/j.epsl.2022.117651
- Nesbit, P. R., Boulding, A. D., Hugenholtz, P. H., Durkin, P. R., and Hubbard, S. M. (2020). Visualization and sharing of 3D digital outcrop models to promote open science. *GSA Today* 30 (6), 4–10. doi:10.1130/GSATG425A.1
- Ori, G. G., and Friend, P. (1994). Sedimentary basins formed and carried piggy-back on active thrust sheets. *Geology* 12 (4), 475–478. doi:10.1130/0091-7613(1984)12<475:sbfacp>2.0.co;2
- Ouyed, M., Idres, M., Bourmatte, A., Boughacha, M. S., Samai, S., Yelles, A., et al. (2011). Attempt to identify seismic sources in the eastern Mitidja basin using gravity data and aftershock sequence of the Boumerdes (May 21, 2003; Algeria) earthquake. *J. Seismol.* 15, 173–189. doi:10.1007/s10950-010-9218-3
- Palano, M., González, P. J., and Fernández, J. (2015). The diffuse plate boundary of nubia and iberia in the western mediterranean: Crustal deformation evidence for viscous coupling and fragmented lithosphere. *Earth Planet. Sci. Lett.* 430, 439–447. doi:10.1016/j.epsl.2015.08.040
- Perea, H., Martínez-Lorienté, S., Maloney-Maesano, F. E., and Vannucchi, P. (2021). Editorial: Submarine active faults: From regional observations to seismic hazard characterization. *Front. Earth Sci.* 9. doi:10.3389/feart.2021.809205
- Pettinga, L. A., and Jobe, Z. R. (2021). How submarine channels (re)shape continental margins. *J. Sediment. Res.* 90 (11), 1581–1600. doi:10.2110/jsr.2020.72
- Pfiffner, O. A. (2017). Thick-skinned and thin-skinned tectonics: A global perspective. *Geosci. Switz.* 7 (71), 71–89. doi:10.3390/geosciences7030071
- Polonia, A., Torelli, L., Mussoni, P., Gasperini, L., Artoni, A., and Klaeschen, D. (2011). The Calabrian Arc subduction complex in the Ionian Sea: Regional architecture, active deformation, and seismic hazard. *Tectonics* 30, TC5018. doi:10.1029/2010TC002821
- Pratson, L. F., Nittrouer, C. A., Wiberg, P. L., Steckler, M. S., Swenson, J. B., Cacchione, D. A., et al. (2007). "Seascape evolution on clastic continental shelves and slopes," in *Continental margin sedimentation: From sediment transport to sequence stratigraphy*. Editors C. A. Nittrouer, J. A. Austin, M. E. Field, J. H. Kravitz, J. P. M. Syvitski, and P. L. Wiberg (Gent, Belgium: Special Publications of the International Association of Sedimentology), Vol. 37, 340–380.
- Ratzov, G., Cattaneo, A., Babonneau, N., Déverchère, J., Yelles, K., Bracene, R., et al. (2015). Holocene turbidites record earthquake supercycles at a slow-rate plate boundary. *Geology* 43, 331–334. doi:10.1130/G36170.1
- Raymond, D. (1976). *Evolution sédimentaire et tectonique du Nord-Ouest de la Grande Kabylie (Algérie) au cours du cycle alpin*. Paris, France: Thèse d'état, Université Pierre et Marie Curie, 160.
- Recanati, A., Missenard, Y., Leprêtre, R., Gautheron, C., Barbarand, J., Abbassene, F., et al. (2019). A Tortonian onset for the Algerian margin inversion: Evidence from low-temperature thermochronology. *Terra nova.* 31 (1), 39–48. doi:10.1111/ter.12367
- Roveri, M., Flecker, R., Krijgsman, W., Lofi, J., Lugli, S., Manzi, V., et al. (2014). The Messinian Salinity Crisis: Past and future of a great challenge for marine sciences. *Mar. Geol.* 352, 25–58. doi:10.1016/j.margeo.2014.02.002
- Sage, F., Beslier, M.-O., Thinon, I., Larroque, C., Dessa, J. X., Migeon, S., et al. (2011). Structure and evolution of a passive margin in a compressive environment: Example of the south-Western Alps-Ligurian basin junction during the Cenozoic. *Mar. Petroleum Geol.* 28 (7), 1263–1282. doi:10.1016/j.marpetgeo.2011.03.012
- Savoye, B., and Piper, D. J. W. (1991). The Messinian event on the margin of the Mediterranean sea in the Nice area, southern France. *Mar. Geol.* 97, 279–304. doi:10.1016/0025-3227(91)90121-j
- Serpelloni, E., Cavaliere, A., Martelli, L., Pintori, F., Anderlini, L., Borghi, A., et al. (2022). Surface velocities and strain-rates in the Euro-Mediterranean Region from massive GPS data processing. *Front. Earth Sci.* 10, 907897. doi:10.3389/feart.2022.907897
- Serpelloni, E., Vannucci, G., Pondrelli, S., Argani, A., Casula, G., Anzidei, M., et al. (2007). Kinematics of the Western Africa-Eurasia plate boundary from focal mechanisms and GPS data. *Geophys. J. Int.* 169 (3), 1180–1200. doi:10.1111/j.1365-246X.2007.03367.x
- Shepard, F. P. (1981). Submarine canyons: Multiple causes and long-time persistence. *Am. Assoc. Petroleum Geol. Bull.* 65, 1062–1077.
- Somoza, L., Medialdea, T., Terrinha, P., Ramos, A., and Vázquez, J. T. (2021). Submarine active faults and morpho-tectonics around the Iberian margins: Seismic and tsunamis hazards. *Front. Earth Sci.* 9, 653639. doi:10.3389/feart.2021.653639
- Sparacino, F., Palano, M., Peláez, J. A., and Fernández, J. (2020). Geodetic deformation versus seismic crustal moment-rates: Insights from the iberomaghrebian region. *Remote Sens.* 12 (6), 952. doi:10.3390/rs12060952
- Strzeczynski, P., Déverchère, J., Cattaneo, A., Domzig, A., Yelles, K., Mercier de Lépinay, B., et al. (2010). Tectonic inheritance and Pliocene-Pleistocene inversion of the Algerian margin around Algiers: Insights from multibeam and seismic reflection data. *Tectonics* 29, TC2008. doi:10.1029/2009tc002547
- Strzeczynski, P., DominguezBoudiaf, A., Déverchère, J., and Deverchere, J. (2021). Tectonic inversion and geomorphic evolution of the Algerian margin since messinian times: Insights from new onshore/offshore analog modeling experiments. *Tectonics* 40, e2020TC006369. doi:10.1029/2020TC006369
- Suppe, J. (1983). Geometry and kinematics of fault-bend folding. *Am. J. Sci.* 283 (7), 684–721. doi:10.2475/ajs.283.7.684
- Xiao, H., and Suppe, J. (1992). Origin of rollover. *AAPG Bull. Am. Assoc. Petroleum Geol.* 76 (4), 509–529.
- Yelles-Chaouche, A., Boudiaf, A., Djellit, H., and Bracene, R. (2006). *Active tectonics in northern Algeria*. doi:10.1016/j.crte.2005.11.002